

Extended body motion in the 2 and 3-body problem

Michael Gaffney
B.Sc.

A thesis submitted for the degree of Master of Science

Dublin City University

Supervisor:

Dr. Abraham Harte

Centre for Astrophysics and Relativity

School of Mathematical Sciences

Dublin City University

January 2022

Declaration

I hereby certify that this material, which I now submit for assessment on the programme of study leading to the award of Master of Science is entirely my own work, and that I have exercised reasonable care to ensure that the work is original, and does not to the best of my knowledge breach any law of copyright, and has not been taken from the work of others save and to the extent that such work has been cited and acknowledged within the text of my work.

Signed: 

ID Number: 15496638

Date: 12 January 2022

Acknowledgements

I would first like to thank my supervisor, Abraham Harte for all his help and most importantly, his patience over the past three years! Thank you also to everyone in CfAR and the School of Maths for welcoming me, even as an outsider from physics.

I would also like to thank my friends, especially Caitlin and Shane for all the laughs and encouragement, I definitely couldn't have done it without you. And finally, thank you to my parents for everything you've done for me, in particular your constant support and to my nana, for being my biggest supporter!

Contents

List of Figures	vi
Abstract	viii
1 Introduction	1
1.1 Propulsion technologies	1
1.2 Extended spacecraft	2
1.3 Outline	5
2 Motion in general gravitational fields	7
2.1 2-body problem	8
2.1.1 Energy	11
2.1.2 Force	14
2.1.3 Torque	15
2.1.4 Precession	15
2.2 3-body problem	18
2.2.1 Force and torque	20
2.2.2 Planar, circularly restricted 3-body problem	21
2.2.3 Jacobi constant	22
2.2.4 Lagrange points	24
2.2.5 Hill region	27

3	Results	30
3.1	2-body problem	30
3.1.1	Torque-free extended spacecraft	30
3.1.2	Changing energy and eccentricity	32
3.1.3	Controlling the precession	41
3.1.4	Example extended spacecraft	44
3.1.5	Numerical examples	49
3.2	3-body problem	50
3.2.1	Gravitational force and torque	51
3.2.2	Non-dimensionalised equations of motion	52
3.2.3	Change in Jacobi constant	55
3.2.4	Orbits to decrease Jacobi constant	57
3.2.5	Numerical results for 2-body limit	60
3.2.6	Numerical results for low mass ratio	67
3.2.7	Controlling the precession	69
3.2.8	Stabilising	71
3.2.9	Numerics	75
4	Conclusions	81
4.1	Discussion	81
4.1.1	2-body problem	82
4.1.2	3-body problem	83
4.2	Future perspectives	85
	Bibliography	87

List of Figures

2.1	Closed, elliptic orbit in the Kepler problem	17
2.2	Example elliptic orbits of a spacecraft precessing due to some perturbative force	18
2.3	Lagrange points for the restricted 3-body problem	25
2.4	Hill regions corresponding to five different values of C	28
3.1	Effective potential curves for two values of q	35
3.2	Increase in eccentricity using cyclic changes in q to increase energy	38
3.3	Decrease in pericentre using cyclic changes in q to increase energy	40
3.4	Orbits of an extended spacecraft using eccentricity increasing strategy	40
3.5	Non-precessing orbits of spacecraft with eigenvalues sum equal to zero	45
3.6	Decrease in Jacobi constant using changes in q	56
3.7	Maximum initial position with range of initial r_0 with initial Hill region for this system	59
3.8	Number of orbits for $C = C_1$ with $\mu = 0$	61

3.9	Initial eccentricity against the initial radius for some value of C_0	64
3.10	Numerical and analytic results for number of orbits to decrease $C = C_1$	65
3.11	Number of orbits for $C = C_1$ with $\mu = 0.01$	68
3.12	Example orbits showing how strategically choosing the sum of the eigenvalues ensures the orbit does not precess	70
3.13	Potential curves for $q > 0$, $q < 0$ and $q = 0$, showing the corresponding unstable equilibrium point for each curve	73
3.14	Hill region about L_1 for an extended spacecraft with C slightly greater than C_1 , with $q = 0$, $q > 0$ and $q < 0$.	74
3.15	Orbits of an extended spacecraft within a Hill region about L_1 , created by switching the sign of q either side of the equilibrium point	75
3.16	Difference between analytical and numerical data for number of orbits, while changing accuracy and precision goal	77
3.17	Difference between analytical and numerical data using a fixed step, Explicit Runge Kutta of order 2 for the integration method for <i>NDSolve</i> , while varying the step size	78
3.18	Difference between the position of the spacecraft after 10 time units and the same value found while changing the accuracy and precision goals in <i>NDSolve</i>	79
3.19	Difference between the position of the spacecraft after 10 time units, found using automatic method and tolerances, and the same value found by varying the step size using fixed step, Ex- plicit Runge Kutta integration method in <i>NDSolve</i>	80

Abstract

Extended body motion in the 2 and 3-body problem

Michael Gaffney

Orbital mechanics is most often concerned with the trajectories of point particles. These trajectories are fixed given some initial position and velocity but are most often changed by firing a rocket. However, by stepping away from the point particle approximation and now considering an extended spacecraft, it will be shown that changes can be made to its orbit, without the use of a reaction mass. By strategically varying the spacecraft's mass distribution, it can, over time, result in large changes to the spacecraft's orbit in the 2 and 3-body problem. Doing this can allow for an extended spacecraft to perform fuel-free orbital manoeuvres such as transferring its orbit from one primary body to another or to escape the 3-body system.

In contrast to much of the current literature, here we do not adopt a model for the extended spacecraft and more importantly, show how some general extended spacecraft can be torque-free by requiring that the radial vectors from the primary bodies are eigenvectors of the quadrupole moment of the spacecraft's mass distribution. To the author's knowledge, keeping the spin angular momentum constant by ensuring the radial vectors are eigenvectors of the quadrupole moment has not been demonstrated before.

We show that the change in energy and Jacobi constant is proportional to the difference in the minimum and maximum of the eigenvalue of the quadrupole moment. It is also shown that the sum of the minimum and maximum eigenvalue is proportional to the precession of the orbit as a result of the spacecraft being an extended body and this can be used to offset the precession induced in the 3-body problem.

Finally, it is shown that changing the sign of the eigenvalue either side of an unstable equilibrium can allow for an extended spacecraft to stabilise itself about otherwise unstable points. The saddle point of Lagrange point 1 was used as an example to also show numerically that strategically changing the sign of the eigenvalue either side of L_1 stabilises the spacecraft in the region about the equilibrium point.

Chapter 1

Introduction

During the Mongol siege of Kai-Keng, China in 1232, rockets were first recorded being used as weapons to propel fire arrows at the hordes of invaders. The use of gunpowder as a propellant then spread across Europe and Asia between the 13th and 16th century. Most of the recorded uses of gunpowder during this time was for warfare but the first story of using rockets to travel into space came in the 16th century. Wan Hu, a Chinese astronomer wishing to travel to the Moon, assembled a chair, attached to which were 47 gunpowder rockets. With the help of his assistants, the rockets were lit, and after the subsequent explosion and the smoke had cleared, Wan Hu had disappeared. The story goes that he made it into space and that you can see him now as the “Man on the Moon” [1]! It is clear that since Wan Hu’s efforts, developing and creating improved propulsion methods for use in space has been at the forefront of rocket science.

1.1 Propulsion technologies

In general, a spacecraft wishing to change or maintain its orbit will fire a rocket by expelling a reaction mass. The rocket produces thrust as described by

Newton's third law of motion [2]. Expelling a reaction mass requires a rocket to carry fuel which is of course, a finite resource in space. The specific impulse of a reaction mass rocket is used as a measure of how efficiently the rocket produces thrust. The higher the specific impulse of a rocket, the more efficiently it uses fuel to generate thrust [3]. Most rockets use chemical propulsion systems which generate thrust through chemical reactions to heat a gas which is then expanded [4]. However, the specific impulse of chemical rockets is quite low and so more recently, electric propulsion and specifically ion thrusters, have been used for orbital adjustments and maintaining an orbit [5–7]. Although ion thrusters have much a higher specific impulse, it still requires fuel and when these spacecraft run out of fuel, they can no longer control it's orientation so as to communicate with Earth, or to face its solar panels towards the Sun to recharge and so the mission must be ended [8].

There has also been extensive research into alternative methods of changing and maintaining a spacecrafts orbit without the need for fuel. One such method is solar sail propulsion which generates thrust from the radiation pressure exerted by the light from a star on the sail [4]. The total force exerted on an ideal, square sail of area $1km^2$ at a distance of $1AU$ from the Sun is approximately $9N$ making it a low thrust propulsion system but given time, can be sufficient to be used to perform orbital adjustments. The force exerted on the sail varies by the inverse square of the distance to the star, and by the square of the cosine of the angle of incidence of the light on the sail [9].

1.2 Extended spacecraft

Another fuel-free propulsion method involves manoeuvring a spacecraft using extended body effects. Controlling the mass distribution of a spacecraft subsequently allows it to control the gravitational force and torque being exerted on it. Controlling the mass distribution of the spacecraft does of course, require some energy but this energy could be acquired from some source, for example using solar panels and batteries, as opposed to a finite fuel reserve.

The spacecraft could use this chemical energy from the battery or some other internal energy, and convert it to the spacecraft's orbital energy in some way. Therefore, fuel-free manoeuvres are those not requiring the use of a reaction mass to make changes to the spacecraft's orbit.

While extended body effects only change the force slightly, given some time, fuel-free manoeuvres are possible. This has been discussed before, usually by adopting a model of a spacecraft consisting of two point masses connected by a tether [10–15]. There have also been a number of in-flight demonstrations for the feasibility of tethers in space, such as the retrieval of a tether during the Tethered Satellite System mission, TSS-1, in 1992 and during the Small Expendable Deployer System, SEDS-1, where a tether was deployed at a length of $20km$ [4, 16]. In practice, these missions involving a tethered spacecraft used a current carrying, electrodynamic tether which generates thrust from a magnetic field exerting a force on the tether [4]. It has also been proposed to use an electrodynamic tether to maintain the orbit of the spacecraft near one of the Lagrange points of an inner moonlet of Jupiter, while also generating power to meet the energy requirements of a scientific observatory [17, 18].

As mentioned, much of the research exploring extended body effects adopts model of a barbell spacecraft. We instead choose to study extended body motion much more generally, without adopting a particular model for the extended spacecraft. Research into extended spacecraft have also had various ideas as to how to deal with the torque exerted on the spacecraft, such as using a reaction wheel to control the spacecrafts orientation [13, 14]. In spherically symmetric gravitational fields, the total angular momentum, \mathbf{L} , is conserved and is equal to the sum of the orbital angular momentum, \mathbf{L}_{orb} and spin angular momentum, \mathbf{L}_{spin} . Some research allows for a transfer of angular momentum from orbital to spin and back, such that $\dot{\mathbf{L}}_{spin} = -\dot{\mathbf{L}}_{orb}$ [10, 12]. However, even a small change in the orbital angular momentum would lead to a change in the spin angular momentum large enough so that the spacecraft could tear itself apart and this will be discussed in section 3.1.1.

To overcome this issue of the spacecraft spinning up, we choose to keep

the spin angular momentum constant. To ensure the torque exerted on the spacecraft vanishes, we will see that the radial vector must be an eigenvector of the quadrupole moment of the spacecraft's mass distribution, the mathematical definition for which will be given in equation (2.6), where \mathbf{z} is the centre of mass position. To the author's knowledge, keeping the spin angular momentum constant by ensuring the radial vectors are eigenvectors of the quadrupole moment has not been demonstrated before and more detail is provided in section 2.1.

Due to the degeneracy of two of the eigenvalues of the quadrupole moment, in the 3-body problem, both radial vectors can simultaneously be eigenvectors of the quadrupole moment. Therefore, the torque exerted on extended spacecraft will vanish once again, even with two primary bodies exerting a torque. With the radial vectors being eigenvectors of the quadrupole moment, the eigenvalue, q becomes the relevant control parameter of the spacecraft. Strategically varying the sign and magnitude of this eigenvalue allows an extended body spacecraft to perform some fuel-free orbital manoeuvres without the need for a reaction mass.

There are a number of ideas discussed in this thesis which, to the author's knowledge, have not been discussed or demonstrated before. This includes not adopting a particular model for the extended spacecraft and instead here we choose to look at some general extended body and study its quadrupole moment. As mentioned, instead of using a reaction wheel or allowing a conversion of spin angular momentum and orbital angular momentum, here we show that the torque exerted on the spacecraft vanishes by ensuring the radial vector must be an eigenvector of the quadrupole moment of the spacecraft's mass distribution. This is discussed in sections 3.1.1 and 3.2.1.

This problem has also been analysed extensively in the 2-body problem but in the 3-body problem, this is not the case. In [18], they discuss the use of an electrodynamic tethered spacecraft to stabilise its orbit in Jupiter's plasmasphere. However, we again choose to look at a more general extended spacecraft which does not rely on electrodynamic effects to stabilise its or-

bit and also show how this general extended spacecraft can be used to make changes to its orbit, without the use of a reaction mass and this is discussed in section 3.2. Finally, investigations into motion in the 3-body problem usually involve using a computer to solve the equations of motion numerically. While this is also done here, in addition, we look at the changes in energy in the 2-body problem and in Jacobi constant in the 3-body problem, and show how these changes relate to changes in the mass distribution of the extended spacecraft. The 2-body problem is discussed in this context in section 3.1.2 and changes in energy are shown in figure 3.1. Then changes in the Jacobi constant are discussed in section 3.2.3 and shown in figure 3.6.

1.3 Outline

This thesis studies the motion of an extended body spacecraft in the 2 and 3-body problem. Extended body effects can be used to change a spacecrafts orbit or to stabilise about an unstable equilibrium point. These manoeuvres can be performed without the use of rockets and are therefore fuel-free manoeuvres. Although extended body effects differ only slightly from the point particle equivalent, given enough time, large changes can be achieved by those who wait! Motion in general gravitational fields for an extended body is discussed in chapter 2, by deriving expressions for the energy, force, torque and precession angle in terms of the quadrupole moment of the mass distribution of the body. Then, similar equations for the force and torque are developed for the 3-body problem and the concepts required to analyse the motion of an extended body are also introduced.

Chapter 3 outlines the main results for an extended body spacecraft in the 2 and 3-body problem. An important problem to overcome is that for an extended spacecraft, a primary body can exert a torque which leads to the spacecraft spinning up and could eventually tear itself apart. To ensure the torque exerted on an extended spacecraft vanishes, we see that the radial vectors of the spacecraft must be eigenvectors of the quadrupole moment, for some

eigenvalue associated with the eigenvector. This eigenvalue is time dependent and as mentioned, is the relevant control parameter for an extended spacecraft. It is shown that by strategically changing the value of this eigenvalue of the quadrupole moment, the orbital energy and the eccentricity of the orbit can be changed.

Then, in the 3-body problem, once again, using a strategy for changing the eigenvalue, a torque-free extended spacecraft can change the value of its Jacobi constant. This can eventually lead to the possibility of orbital transfers between primary bodies. The sum of the minimum and maximum eigenvalues of the quadrupole moment can also be used to control the precession of the extended spacecrafts, allowing for the spacecraft to more easily pass through a gap in the Hill region.

The ability of an extended spacecraft to stabilise itself about an unstable point is also investigated. It is shown numerically that using a control law for the sign of the eigenvalue allows for an extended spacecraft to remain in the enclosed Hill region about an unstable equilibrium point, such as Lagrange point 1.

Finally, in chapter 4, the main results of the thesis are discussed and areas for future research are suggested and discussed briefly. Areas where the current work could be improved and made more precise, along with other problems in which the motion of an extended spacecraft could be investigated, are also identified.

Chapter 2

Motion in general gravitational fields

Orbital mechanics is most often concerned with the orbits of point particle objects, which of course is only an approximation. In reality primary bodies have some size and can be considered extended bodies. Stars, planets and moons are all extended bodies and this has an affect on their shape and on the orbits of any orbiting bodies. For example, the gravitational force exerted by a planet on a moon causes the moon to become more oblate. This, in turn can lead to the moon becoming tidally locked to the planet, where the rotational period of the moon becomes equal to the orbital period about the planet. This can be seen from the Earth-Moon system, where the Moon is tidally locked to the Earth, or in the case of the Pluto-Charon system, both bodies are tidally locked to each other [19].

As discussed in section 1.1, extended body effects can also arise in spacecraft and can be used to perform some orbital manoeuvres. However, adopting the specific model of a tethered spacecraft can obscure the fundamental physics involved and so here we instead explore the possibilities of extended body effects without adopting a particular model for an extended spacecraft.

2.1 2-body problem

Here, we discuss general gravitational fields, outside their sources, which satisfies Newton's laws of gravity in the form of

$$\mathbf{g} = -\nabla\Phi, \quad \nabla^2\Phi = 0, \quad (2.1)$$

We now consider some general extended spacecraft with mass density $\rho(\mathbf{x}, t)$ and total mass $m = \int \rho d^3\mathbf{x}$. Two important characteristics of an extended spacecraft are its centre of mass position, $\mathbf{z}(t)$ and its spin angular momentum, $\mathbf{S}(t)$. These satisfy $\mathbf{F} = m\ddot{\mathbf{z}}$ and $\dot{\mathbf{S}} = \boldsymbol{\tau}$, where \mathbf{F} is the total force and $\boldsymbol{\tau}$ is the torque. If all forces are gravitational and the spacecrafts gravitational field is sufficiently small, the total gravitational field is just the external gravitational field, \mathbf{g} and then the gravitational force and torque exerted on an extended spacecraft are given by

$$\mathbf{F} = \int \rho \mathbf{g} d^3\mathbf{x}, \quad (2.2)$$

$$\boldsymbol{\tau} = \int \rho(\mathbf{x} - \mathbf{z}) \times \mathbf{g} d^3\mathbf{x}. \quad (2.3)$$

If we assume that the gravitational field varies only slightly throughout the spacecraft, we can Taylor expand the gravitational field for $\mathbf{x}(t)$ close to $\mathbf{z}(t)$. When the size of the spacecraft is small compared to distances to all other bodies, this ensures the gravitational field does vary only slightly. Using Einstein summation convention for repeated indices such that $(x - z)^j \partial_j g_i = \sum_{j=1}^3 (x - z)^j \partial_j g_i$ [20], the expansion of the gravitational field is given by

$$g_i(\mathbf{x}) = g_i(\mathbf{z}) + \partial_j g_i(\mathbf{z})(x - z)^j + \frac{1}{2} \partial_j \partial_k g_i(\mathbf{z})(x - z)^j (x - z)^k + \dots \quad (2.4)$$

Substituting the expansion (2.4) into equation (2.2) and ignoring higher order terms

$$F_i = mg_i + \partial_j g_i \int \rho(x-z)^j d^3\mathbf{x} + \frac{1}{2} \partial_j \partial_k g_i \int \rho(x-z)^j (x-z)^k d^3\mathbf{x} + \mathcal{O}\left(m \left(\frac{l}{R}\right)^3\right),$$

where l denotes the size of the spacecraft and R is the distance to a primary body. The centre of mass position z_i is given by

$$z_i = \frac{1}{m} \int \rho x_i d^3\mathbf{x},$$

we can use this to show the dipole moment of the mass distribution vanishes as shown by

$$\int \rho(x-z)^j d^3\mathbf{x} = (z^j m - z^j m) = 0.$$

Moments of the mass distribution depend on the choice of origin and so the dipole moment can always be made to vanish by choosing z_i in this way. We can then write the force showing the monopole moment, m ,

$$F_i = mg_i + \frac{1}{2} \partial_j \partial_k g_i \bar{Q}^{jk}, \quad (2.5)$$

where \bar{Q}^{ij} is the quadrupole moment of the mass distribution, which is symmetric and can be time dependent, and is given by

$$\bar{Q}^{ij} \equiv \int \rho(x-z)^i (x-z)^j d^3\mathbf{x}. \quad (2.6)$$

The external gravitational field satisfies the Laplace equation, $\nabla^2 \mathbf{g} = 0$ [21], throughout the extended spacecraft meaning the gravitational field is harmonic. As a result, we can use this freedom to add arbitrary multiples of the Kronecker delta, δ^{ij} to \bar{Q}^{ij} without affecting the force or the torque. The trace of the quadrupole moment is therefore irrelevant and as such, we can redefine \bar{Q}^{ij} so as to make it trace-free as shown by

$$Q^{ij} = \bar{Q}^{ij} + \alpha \delta^{ij},$$

To show how arbitrary multiples of $\alpha \delta^{ij}$ can be added to \bar{Q}^{ij} without affecting the force or the torque, we use the substitution for Q^{ij} in (2.5), giving

$$\begin{aligned} F_i &= mg_i + \frac{1}{2} \partial_j \partial_k g_i (\bar{Q}^{jk} + \alpha \delta^{jk}), \\ &= mg_i + \frac{1}{2} \left(\partial_j \partial_k g_i \bar{Q}^{jk} + \alpha \partial_j \partial_k g_i \delta^{jk} \right). \end{aligned}$$

Summing over the repeated indices means two cases arise; the first is when $j \neq k$, which results in $\delta^{jk} = 0$, meaning we are only left with the first term in brackets in the force, which are not affected by adding $\alpha \delta^{ij}$ to \bar{Q}^{ij} . The second case is $j = k$, with $\delta^{jj} = 1$. In this case, the force is

$$F_i = mg_i + \frac{1}{2} \partial_j \partial_j g_i (\bar{Q}^{jj} + \alpha)$$

and we can write the derivatives of g_i as $\partial_j \partial_j g_i = \nabla^2 g_i = 0$, from (2.1).

Now, α is chosen such that the trace of Q^{ij} vanishes, and is given by

$$\alpha \equiv -\frac{1}{3} \int \rho |\mathbf{x} - \mathbf{z}|^2 d^3 \mathbf{x}.$$

Adding α to equation (2.6) gives the symmetric and now trace-free quadrupole moment matrix

$$Q^{ij} \equiv \int \rho \left[(x - z)^i (x - z)^j - \frac{1}{3} \delta^{ij} |\mathbf{x} - \mathbf{z}|^2 \right] d^3 \mathbf{x}. \quad (2.7)$$

Now using Q^{ij} , we arrive at an expression for the force including the symmetric and now trace-free quadrupole moment:

$$F_i = mg_i + \frac{1}{2} \partial_j \partial_k g_i Q^{jk}, \quad (2.8)$$

where once again, the dipole moment vanished due to the choice for the origin and we have ignored higher order terms.

This redefined quadrupole moment can also be used to compute the torque exerted on the extended spacecraft. Starting with equation (2.3) and using the Taylor expanded gravitational field and \bar{Q}^{ij} , we can now write the torque as

$$\begin{aligned} \tau_i &= \int \rho (x - z)^j \epsilon_{ijk} (g^k + (x - z)^l \partial_l g^k + \dots) d^3 \mathbf{x}, \\ &= \epsilon_{ijk} \left(g^k \int \rho (x - z)^j d^3 \mathbf{x} + \partial_l g^k \int \rho (x - z)^j (x - z)^l d^3 \mathbf{x} \right), \\ &= \epsilon_{ijk} \partial_l g^k \bar{Q}^{jl}, \end{aligned}$$

where \bar{Q}^{jl} is given by equation (2.6) and the Levi-Civita symbol, ϵ_{ijk} is used such that $(\mathbf{a} \times \mathbf{b})_i = \epsilon_{ijk} a^j b^k$, for any vectors \mathbf{a} and \mathbf{b} . The first integral in the second line vanishes using the centre of mass condition from before. Here, \bar{Q}^{ij} is replaced by Q^{ij} as recalling from equation (2.1), we see that $\partial_l g^k = -\partial_k \partial_l \Phi$ and as the order of the derivatives is irrelevant, $\partial_l g^k$ is a symmetric matrix meaning we can write the torque in terms of Q^{ij} as

$$\tau_i = \epsilon_{ijk} \partial_l g^k Q^{jl} \quad (2.9)$$

In general, the symmetric, trace-free quadrupole moment is given by equation (2.7) but this vanishes when the extended spacecraft is spherically symmetric. This can be seen by starting with the definition of Q^{ij} in equation (2.7). The density of the spherically symmetric spacecraft is some function of the radius, $\rho(r, t)$, the term $(x - z)_i$ is the difference between any point on the spacecraft and the centre of mass. If we define $d_i = (x - z)_i$ and convert to spherical coordinates, we can write

$$\begin{aligned}d_1 &= r \cos \phi \sin \theta, \\d_2 &= r \sin \phi \sin \theta, \\d_3 &= r \cos \theta, \\dx dy dz &= r^2 \sin \theta dr d\phi d\theta,\end{aligned}$$

allowing the quadrupole moment to be written as

$$Q_{ij} = \int \int \int \rho(r) \left(d_i d_j - \frac{1}{3} \delta_{ij} r^2 \right) r^2 \sin \theta dr d\phi d\theta.$$

The radial integral is irrelevant as seen by evaluating the ϕ and θ integrals over the intervals $[0, 2\pi)$ and $[0, \pi]$, respectively, each component of Q_{ij} vanishes resulting in the quadrupole moment of a spherically symmetric spacecraft vanishing. This results in the equations for the force and torque as derived in equations (2.8) and (2.9) to become equal to the equations for a point particle spacecraft, which are given by

$$\mathbf{F} = m\mathbf{g}(\mathbf{z}, t), \quad \boldsymbol{\tau} = 0. \quad (2.10)$$

More generally, the quadrupole moment does not vanish for an extended spacecraft and this will be explored further in this thesis.

2.1.1 Energy

Having derived expressions for the force and torque for an extended spacecraft in terms of Q^{ij} and derivatives of \mathbf{g} for some primary body, we now discuss the orbital energy in the 2-body problem by introducing a scalar gravitational

potential, Φ . We can write this scalar gravitational potential which is related to \mathbf{g} , as

$$\mathbf{g}(\mathbf{z}) = -\nabla\Phi. \quad (2.11)$$

Using this scalar gravitational potential, we can define the ‘point particle orbital energy’ using

$$E_{\text{pt}} \equiv \frac{1}{2}m|\dot{\mathbf{z}}|^2 + m\Phi. \quad (2.12)$$

This is the energy an extended spacecraft could have if it rapidly changed shape so as to make $Q^{ij} = 0$. It can be shown that this is conserved when the gravitational field is static ($\partial\Phi/\partial t = 0$) and when the quadrupole moment is constant. This energy can change if the field is not static or if we allow for extended body effects, as such the time derivative of this energy can be written as

$$\begin{aligned} \dot{E}_{\text{pt}} &= \frac{1}{2}m \frac{d}{dt} (|\dot{\mathbf{z}}|^2) + m \frac{d\Phi}{dt}, \\ &= \frac{1}{2}m(2\dot{z}^i \ddot{z}_i) + m \left(\frac{\partial\Phi}{\partial t} + \dot{z}^i \partial_i \Phi \right), \\ &= \dot{z}^i (m\ddot{z}_i) + m \frac{\partial\Phi}{\partial t} + \dot{z}^i (m\nabla_i \Phi). \end{aligned}$$

The product $m\ddot{\mathbf{z}}$ is the force including the quadrupole moment and the product $m\nabla\Phi$ is equal to the negative of the point particle force. By using equations (2.8) and (2.11), the change of energy in time can be written in terms of the quadrupole moment such that

$$\begin{aligned} \dot{E}_{\text{pt}} &= \dot{z}^i (mg_i + \frac{1}{2}\partial_j \partial_k g_i Q^{jk}) + m \frac{\partial\Phi}{\partial t} - \dot{z}^i (mg_i), \\ &= m \frac{\partial\Phi}{\partial t} + \frac{1}{2}\dot{z}^i \partial_j \partial_k g_i Q^{jk}. \end{aligned} \quad (2.13)$$

Another notion of energy differs from the first if we include the Taylor expanded gravitational potential and not just the point particle potential $m\Phi$, such that

$$\begin{aligned} U &= \int \rho \Phi d^3\mathbf{x}, \\ &= \int \rho \left(\Phi + (x-z)^j \partial_j \Phi + \frac{1}{2}(x-z)^j (x-z)^k \partial_j \partial_k \Phi \right) d^3\mathbf{x}, \\ &= m\Phi - \frac{1}{2}\partial_j g_k Q^{jk}. \end{aligned} \quad (2.14)$$

The first term is the point particle gravitational potential along with the quadrupole moment of the potential. Using this expression for the gravitational potential, we can define another energy in the quadrupole approximation as

$$\begin{aligned}
E &\equiv \frac{1}{2}m|\dot{\mathbf{z}}|^2 + U, \\
&= E_{\text{pt}} - \frac{1}{2}\partial_j g_k Q^{jk}, \\
&= m\Phi + \frac{1}{2}m|\dot{\mathbf{z}}|^2 - \frac{1}{2}\partial_j g_k Q^{jk}.
\end{aligned} \tag{2.15}$$

Neither notion of energy includes internal kinetic or chemical energy and so may not necessarily be conserved as neither are the total energy. As such, taking the time derivative of this energy, again using the chain rule as before,

$$\begin{aligned}
\dot{E} &= \dot{E}_{\text{pt}} - \frac{1}{2} \left(\partial_j g_k \frac{d}{dt} Q^{jk} + Q^{jk} \frac{d}{dt} \partial_j g_k \right), \\
&= m \frac{\partial \Phi}{\partial t} + \frac{1}{2} \dot{z}^i \partial_j \partial_k g_i Q^{jk} \\
&\quad - \frac{1}{2} \left(\partial_j g_k \dot{Q}^{jk} + \dot{z}^i \partial_j \partial_k g_i Q^{jk} + Q^{jk} \frac{\partial}{\partial t} (\partial_j g_k) \right), \\
&= \left(m \frac{\partial \Phi}{\partial t} - \frac{1}{2} Q^{jk} \frac{\partial}{\partial t} (\partial_j g_k) \right) - \frac{1}{2} \partial_j g_k \dot{Q}^{jk},
\end{aligned} \tag{2.16}$$

where the first two terms in the second line are given by equation (2.13). The terms in the brackets vanish when the field is static as $\partial(\partial_i g_j)/\partial t = -\partial_i \partial_j (\partial \Phi / \partial t) = 0$ and this energy is conserved when $\partial_j g_k \dot{Q}^{jk} = 0$. Allowing the extended spacecraft to change its shape and therefore change the quadrupole moment means the energy of the spacecraft can be varied. In an ideal situation, the change in shape of the extended spacecraft occurs instantaneously so using this, we can assume that the changes in the quadrupole moment are discrete. Therefore, in a static field, the change in energy given by equation (2.16) can be written as

$$\delta E = \delta U = -\frac{1}{2} \partial_i g_j \delta Q^{ij}. \tag{2.17}$$

For a point particle, the quadrupole moment is zero and therefore the energy does not change. Now assuming there is a single primary body with a

scalar potential

$$\Phi = -\frac{GM}{|\mathbf{x}|}, \quad (2.18)$$

the discrete change in energy becomes

$$\delta E = -\frac{GM}{2}\delta Q^{ij}\frac{\partial}{\partial x_i}\left(-\frac{1}{|\mathbf{x}|^3}x_j\right),$$

then using the following relations,

$$\frac{\partial}{\partial x_j}x_i = \delta_{ij}, \quad \frac{1}{|\mathbf{x}|^3} = (x_i^2)^{-\frac{3}{2}}, \quad \hat{x}_i = \frac{x_i}{|\mathbf{x}|},$$

we can evaluate the derivative of the gravitational field and as such, δE can be written as

$$\begin{aligned} \delta E &= \frac{GM}{2|\mathbf{z}|^3}\delta Q^{ij}\delta_{ij} - \frac{3GM}{2|\mathbf{z}|^5}\delta Q^{ij}z_iz_j, \\ &= -\frac{3GM}{2|\mathbf{z}|^3}\delta Q^{ij}\hat{z}_i\hat{z}_j, \end{aligned}$$

where the first term, in the first line vanishes as $Q^{jk}\delta_{jk} = \text{tr}(Q^{jk}) = 0$. In these expressions, z_i is the centre of mass position of the extended spacecraft, where we used some expressions involving the centre of mass position, z_i ,

$$r \equiv |\mathbf{z}|, \quad \hat{\mathbf{z}} = \frac{\mathbf{z}}{r}.$$

Having evaluated the discrete change in energy in terms of discrete changes in Q^{ij} , at the centre of mass, we can write

$$\delta E = -\frac{3GM}{2r^3}\hat{z}_j(\delta Q^{ij}\hat{z}_i). \quad (2.19)$$

2.1.2 Force

Once again, we start by using the scalar potential introduced in equation (2.18) to replace \mathbf{g} in the gravitational force, equation (2.8). Now evaluating the derivatives of the gravitational field using the product rule and the same relations as used when evaluating the derivatives in the change in energy, the force can then be written as

$$\begin{aligned} F_i &= mg_i - \frac{1}{2}GMQ^{jk}\frac{\partial}{\partial x_j}\left(-3x_ix_k\frac{1}{|\mathbf{x}|^5} + \delta_{ik}\frac{1}{|\mathbf{x}|^3}\right), \\ &= mg_i + \frac{3GM}{2|\mathbf{x}|^4}Q^{jk}(\delta_{jk}\hat{x}_i + \delta_{ik}\hat{x}_j + \delta_{ij}\hat{x}_k - 5\hat{x}_i\hat{x}_j\hat{x}_k), \end{aligned}$$

where \boldsymbol{x} is the position of some generic point on the extended spacecraft to the primary body. From this point, some further simplifications can be made by looking at the contractions of the quadrupole moment and the Kronecker delta. The first such contraction vanishes as the quadrupole moment is trace-free. The second and third contractions in the brackets are equal which can be seen by summing the repeated indices and then reordering the indices on the right hand side such that $Q^{jk}\delta_{ik}\hat{x}_j = Q^{ij}\hat{x}_j = Q^{ik}\hat{x}_k$. Using these simplifications and evaluating the force at the centre of mass position, we can write the force as

$$F_i = mg_i(z) + \frac{3GM}{r^4} \left(Q_{ij}\hat{z}^j - \frac{5}{2}(Q^{jk}\hat{z}_j\hat{z}_k)\hat{z}_i \right). \quad (2.20)$$

2.1.3 Torque

Using the same arguments as before, we now substitute the scalar potential from (2.18) into the expression for the torque. Starting with equation (2.9), we evaluate the single derivative to give

$$\begin{aligned} \tau_i &= GM\epsilon_{ijk}Q^{jl}\frac{\partial}{\partial x_l} \left(-\frac{1}{|\boldsymbol{x}|^3}x^k \right), \\ &= -\frac{GM}{|\boldsymbol{x}|^3}\epsilon_{ijk} \left(Q^{jl}\delta_{kl} - 3Q^{jl}\hat{x}^k\hat{x}_l \right), \\ &= -\frac{GM}{|\boldsymbol{x}|^3}\epsilon_{ijk} \left(Q^{jk} - 3Q^{jl}\hat{x}^k\hat{x}_l \right). \end{aligned}$$

Now distributing the terms in the brackets and since Q^{ij} is symmetric and ϵ_{ijk} is anti-symmetric, the contraction of the two vanishes such that $Q^{ij}\epsilon_{ijk} = 0$. From this we arrive at another expression for the torque, now evaluated at the centre of mass position.

$$\tau_i = -\frac{3GM}{r^3}\epsilon_{ijk}\hat{z}^j \left(Q^{kl}\hat{z}_l \right). \quad (2.21)$$

2.1.4 Precession

The problem of motion of a pointlike test particle with a force exerted on it given by equation (2.10) is called the Kepler problem. This is an example of

an inverse-square, central force problem, with

$$\mathbf{F} = -kr^n \hat{\mathbf{z}}, \quad (2.22)$$

where in this case, $n = -2$ and $k = GMm$. Bertrand's theorem states that the only central force laws that allow closed orbits are the inverse square law and Hooke's law, where in (2.22), $n = 1$. Therefore, orbits in the Kepler problem are closed as $n = -2$ and as a result, eccentric orbits will not precess, as shown in figure 2.1 [22, 23]. In this figure, a primary body is at a focus of the elliptic orbit. The closest approach of the spacecraft to the primary body is the pericentre, r_p , of the orbit and the furthest point is the apocentre, r_a . The elongation of an ellipse is measured by its eccentricity, e and the diameter in the direction in which the ellipse is elongated is the major axis. Half this diameter is the semi-major axis, a [24].

The Laplace-Runge-Lenz (LRL) vector can be used to describe the precession of an orbit, given by

$$\mathbf{A} \equiv \frac{\dot{\mathbf{z}} \times \mathbf{L}}{GMm} - \frac{\mathbf{z}}{r}, \quad (2.23)$$

where \mathbf{L} is the total angular momentum. The LRL vector is sometimes referred to as the eccentricity vector. In the Kepler problem, this vector is constant and points from the origin of the system to the instantaneous pericentre of the spacecrafts orbit, with magnitude equal to the eccentricity [23].

We now consider a spacecraft which has a force given by equation (2.22) exerted on it but now with some other perturbative force also being exerted on the spacecraft. Now in this problem, Bertrand's theorem implies that if the orbit of a spacecraft is eccentric, it is not closed and therefore the orbit, and the pericentre, will precess. This can be seen in figure 2.2, where a spacecraft has a force exerted on it equal to equation (2.10) with some perturbative force also being exerted. The black dashed arrow shows the precession of the pericentre. Now in this case, the LRL vector is not constant but its magnitude can still be used to define an instantaneous eccentricity such that $e \equiv |\mathbf{A}|$. The direction of \mathbf{A} points from the origin to the instantaneous pericentre of a spacecrafts orbit.

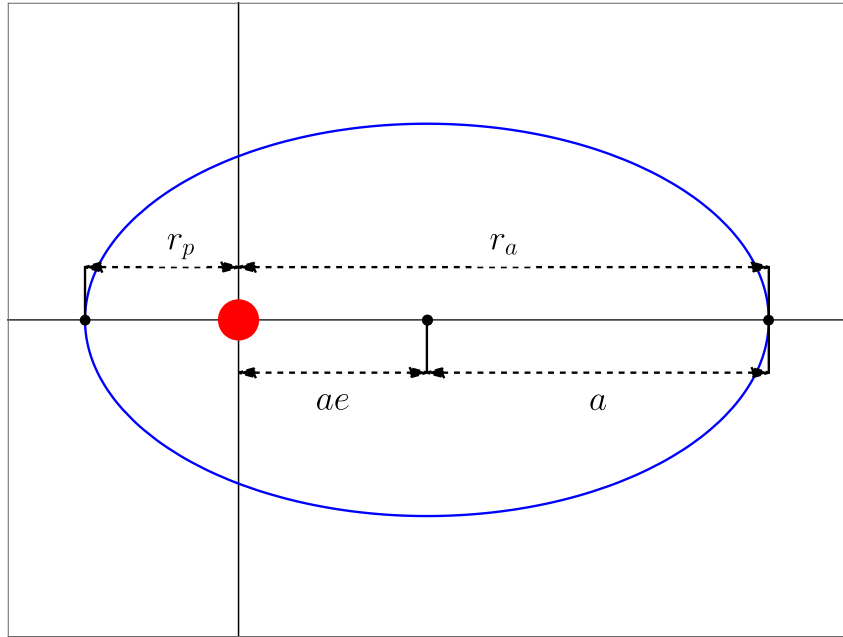


Figure 2.1: Closed, elliptic orbit in the Kepler problem. The primary body is shown in red, with an example orbit of a spacecraft with a force equal to (2.22), where $n = -2$, being exerted on it. The closest approach of the spacecraft to the primary body is the pericentre, shown as r_p and the furthest the spacecraft is from the primary body is the apocentre, r_a . Half the diameter of the ellipse is the semi-major axis, a and the product of this and the eccentricity of the orbit can be used to calculate the distance between the centre of the ellipse and the primary body at a focus, as shown by the distance ae .

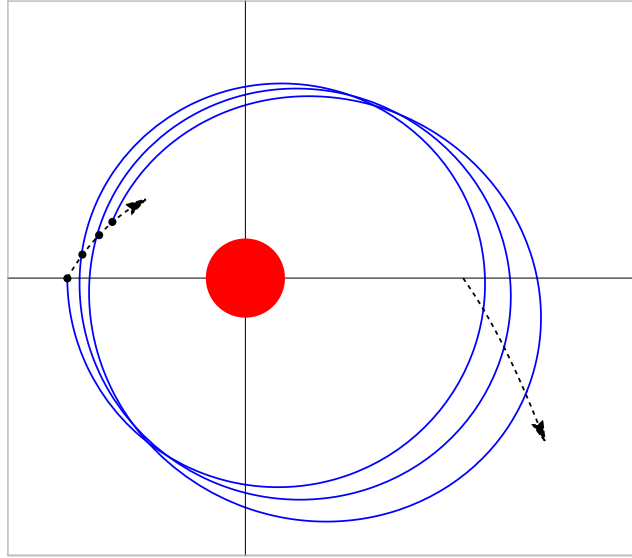


Figure 2.2: Example elliptic orbits of a spacecraft with force equal to (2.22) being exerted on it as well as some perturbative force, or some force equal to (2.22), with $n \neq 2$. Bertrand's theorem implies that this eccentric orbit will precess which can be seen by the black, dashed arrow showing the precession of the pericentre and apocentre. The black points show the location of the instantaneous pericentres.

Examples of this can be seen in the motion of planets in the Solar System. This precession can come from perturbative forces from other planets and also from general relativity. Corrections to Newtonian mechanics found from Einstein's theory of general relativity were able to explain the discrepancies in the precession of the orbit of Mercury [20].

2.2 3-body problem

The 3-body problem was first introduced by Newton, where he studied the motion of the Earth and Moon around the Sun [25]. Newton stated that the problem was difficult to solve although he obtained an approximate solution which agreed with observations to within 8% [26]. Difficulty in deriving solutions arise from the fact that the 3-body problem is chaotic and numerical methods are generally needed to analyse the motion of a body in this system.

Analysis in this problem is commonly focused on the motion of point-like test particles under the influence of two large primary bodies. As will be studied later in this thesis with an extended spacecraft, a point particle spacecraft may wish to transfer its orbit from one primary body to another, or for deep space missions, combine multiple transfers to travel to more distant planets [27]. Transferring between two primary bodies can be done using high or low thrust propulsion systems, where high thrust is based on short burns to change the spacecrafts velocity and low thrust involves smaller but more continuous control. For propulsion systems, the changes in velocity, Δv , are proportional to the change in mass, for small Δm , due to the spacecraft burning fuel. Therefore, missions are designed so as to minimise Δv and the amount of fuel needed [28].

Another application of propulsion systems in space is to maintain the orbit of a spacecraft [29]. Doing this requires regular station keeping meaning a spacecraft must fire a rocket to correct its orbit and which requires fuel. As mentioned in section 1.1, there has been much research in recent years to develop propulsion methods which use fuel more efficiently or do not require fuel.

An extended spacecraft can be used to maintain its orbit using inert and electrodynamic tethers. This has been explored extensively in [18] where a mission to one of Jupiters moons, Io, was designed so as to produce the energy required for a scientific mission. The mission would involve an electrodynamic tethered spacecraft being placed at a Lagrange point of the Jupiter-Io system, where it maintains its stability using extended body effects and produces energy from Jupiters plasmasphere. This, of course, like much of the research into extended body effects in the 2-body problem, adopts a particular model for the tethered spacecraft.

2.2.1 Force and torque

Having derived expressions for the force and torque exerted on an extended spacecraft by one primary body, we can use these same expressions to show the force and torque exerted by two primary bodies, in the 3-body problem. We start with equations (2.8) and (2.9), only now, the gravitational field, g_i is the sum of the gravitational fields from the two primary bodies, such that $\mathbf{g} = \mathbf{g}_1 + \mathbf{g}_2$, where \mathbf{g}_1 is the gravitational field from the first primary body and similarly, \mathbf{g}_2 is the gravitational field from the second primary body.

By Taylor expanding the gravitational field from both primary bodies we can use the same, trace-free symmetric quadrupole moment matrix as in the 2-body problem, equation (2.7). Even though this depends on x^i and z^i , the combination of $(x - z)^i$ is the distance between a generic point on the spacecraft and its centre of mass position. Therefore, the quadrupole moment is independent of the primary bodies and as such does not require a subscript to denote a primary body.

We then evaluate the derivatives of each gravitational field at the centre of mass position, using the fact that the total gravitational field is the sum of both fields from the two primary bodies. The total gravitational force and torque exerted on an extended spacecraft in the 3-body problem is then given by

$$F_{i,\text{tot}} = mg_{i,1} + \frac{3GM_1}{r_1^4} \left(Q_{ij} \hat{z}_1^j - \frac{5}{2} (Q^{jk} \hat{z}_{j,1} \hat{z}_{k,1}) \hat{z}_{i,1} \right) + mg_{i,2} + \frac{3GM_2}{r_2^4} \left(Q_{ij} \hat{z}_2^j - \frac{5}{2} (Q^{jk} \hat{z}_{j,2} \hat{z}_{k,2}) \hat{z}_{i,2} \right), \quad (2.24)$$

$$\tau_{i,\text{tot}} = -\frac{3GM_1}{r_1^3} \epsilon_{ijk} \hat{z}_1^j (Q^{kl} \hat{z}_{l,1}) - \frac{3GM_2}{r_2^3} \epsilon_{ijk} \hat{z}_2^j (Q^{kl} \hat{z}_{l,2}), \quad (2.25)$$

where the radii from the spacecraft to the primary bodies, with mass M_1 and M_2 , is given by r_1 and r_2 , respectively. Einstein summation convention is used once again and so repeated indices are summed over, now, in the 3-body problem, also using subscripts to denote the primary body of interest. To highlight the difference in indices, the vector $F_{i,1}$ denotes the i^{th} component of the force from the first primary body.

2.2.2 Planar, circularly restricted 3-body problem

The 3-body problem can be stated as three bodies moving in space under their mutual gravitational attraction. The 2-body problem can be solved in closed form by directly integrating the equations of motion. In contrast, the 3-body problem is non-linear and a similar solution does not work [30].

To allow us to more easily analyse the problem of motion in the 3-body problem, a number of assumptions are made. The first is that we assume one of the three bodies has negligible mass such that $m \ll M_{1,2}$ and this is the restricted 3-body problem. The two primary bodies are then assumed to orbit circularly about their centre of mass in a 2-body problem and the spacecraft orbits according to the force given by equation (2.24). This is the circular 3-body problem [21]. Finally, we confine the motion of the third body, the spacecraft, to the orbital plane of the primary bodies and giving us the planar 3-body problem. Combining these three assumptions gives us the planar, circularly restricted 3-body problem

Given the two primary bodies orbit as a 2-body problem and in particular have circular orbits, it is more convenient to analyse the motion of a spacecraft in a rotating frame. The rotating frame rotates with the orbits of the primary bodies and as such, the primary bodies appear stationary.

We can understand how a spacecraft moves in the non-rotating or inertial frame, I , using the equations previously derived for the force. However, when we look at the problem in a rotating frame, R , we must find the forces which dictate how a spacecraft will move. By setting the centre of mass of the primary bodies to be the origin of both frames, and the frame R rotates with constant angular velocity ω , the position vector for a spacecraft is given by

$$\mathbf{r} = X\hat{X} + Y\hat{Y}, \quad (2.26)$$

where \hat{X} and \hat{Y} are perpendicular unit vectors which are rotating in the frame I . The rotating vectors \mathbf{X} and \mathbf{Y} are related to the non-rotating vectors, \mathbf{x} and \mathbf{y} , by $\mathbf{X} = R(\omega t)\mathbf{x}$ and $\mathbf{Y} = R(\omega t)\mathbf{y}$, where $R(\omega t)$ is the rotation matrix. To

find the velocity and acceleration of the spacecraft relative to I , we differentiate equation (2.26) with respect to time. Here, we use the fact that $d\hat{X}/dt = \omega\hat{Y}$ and $d\hat{Y}/dt = -\omega\hat{X}$, and so

$$\begin{aligned}\frac{d\mathbf{r}}{dt} &= \dot{\mathbf{r}} = (\dot{X} - \omega Y)\hat{X} + (\dot{Y} + \omega X)\hat{Y}, \\ \frac{d^2\mathbf{r}}{dt^2} &= \ddot{\mathbf{r}} = (\ddot{X} - 2\omega\dot{Y} - \omega^2 X)\hat{X} + (\ddot{Y} + 2\omega\dot{X} - \omega^2 Y)\hat{Y}.\end{aligned}\tag{2.27}$$

Multiplying the acceleration by the mass, m of the spacecraft, yields the apparent total force exerted on the spacecraft by the two primary bodies in the rotating frame. This can be split in to components of the force in the \hat{X} and \hat{Y} directions which gives the equations of motion in the rotating frame.

$$\begin{aligned}\mathbf{F} &= m\ddot{\mathbf{r}} = m(\ddot{X} - 2\omega\dot{Y} - \omega^2 X)\hat{X} + m(\ddot{Y} + 2\omega\dot{X} - \omega^2 Y)\hat{Y}, \\ \mathbf{F} \cdot \hat{X} &= m\ddot{X} - 2m\omega\dot{Y} - m\omega^2 X, & \mathbf{F} \cdot \hat{Y} &= m\ddot{Y} + 2m\omega\dot{X} - m\omega^2 Y, \\ m\ddot{X} &= F_X + 2m\omega\dot{Y} + m\omega^2 X, & m\ddot{Y} &= F_Y - 2m\omega\dot{X} + m\omega^2 Y.\end{aligned}$$

In these equations of motion, the first terms, $F_{X,Y}$, are the \hat{X} and \hat{Y} components of the gravitational force as given by equation (2.24), the second terms are the components of the coriolis force and the third and final terms are the components of the centrifugal force. From this, we can say that the spacecraft moves in relation to the rotating frame of reference in accordance with Newton's law of motion once the two inertial forces, the coriolis and centrifugal forces, are added [31].

Having derived the equations of motion in the rotating frame in terms of \mathbf{X} and \mathbf{Y} , for convenience from this point on, the vectors \mathbf{x} and \mathbf{y} will be used to represent the *rotating* vectors such that

$$\begin{aligned}m\ddot{x} &= F_x + 2m\omega\dot{y} + m\omega^2 x, \\ m\ddot{y} &= F_y - 2m\omega\dot{x} + m\omega^2 y.\end{aligned}\tag{2.28}$$

2.2.3 Jacobi constant

In the 2-body problem, we showed that the change in energy, due to changes in the shape of an extended spacecraft, was proportional to the changes in the

quadrupole moment, as given by equation (2.19).

Starting from the equations of motion for a spacecraft in a rotating frame, equation (2.28), we can rearrange the expressions so as to allow us to write the gravitational force and the centrifugal force in terms of a new scalar potential function, U . We can use the point particle scalar potential, for each of the two primary bodies, U_1 and U_2 , to get

$$U = -\frac{\omega^2}{2}(x^2 + y^2) + U_1 + U_2, \quad (2.29)$$

$$\begin{aligned} m\ddot{x} - 2m\omega\dot{y} &= F_x + m\omega^2x, & m\ddot{y} + 2m\omega\dot{x} &= F_y + m\omega^2y, \\ \ddot{x} - 2\omega\dot{y} &= -\frac{\partial U}{\partial x}, & \ddot{y} + 2\omega\dot{x} &= -\frac{\partial U}{\partial y}, \end{aligned} \quad (2.30)$$

where x and y represent the position of the spacecraft in the rotating frame.

If we then multiply the equation involving \ddot{x} by \dot{x} and the equation involving \ddot{y} by \dot{y} and then add these equations we derive an expression for the total time derivative of equation (2.29) as shown by

$$\frac{dU}{dt} = \dot{x}\frac{\partial U}{\partial x} + \dot{y}\frac{\partial U}{\partial y} = \dot{x}\ddot{x} + \dot{y}\ddot{y} = \frac{d}{dt}\left(\frac{1}{2}(\dot{x}^2 + \dot{y}^2)\right).$$

This equation can be directly integrated to yield

$$\dot{x}^2 + \dot{y}^2 = 2U - C, \quad (2.31)$$

where C is a constant of integration [28]. This constant is the point particle Jacobi constant and it is the only known conserved quantity in the planar circular restricted 3-body problem [32]. Now, if we allow for extended body effects, we replace the point particle scalar potentials, U_1 and U_2 with (2.14) for each primary body, such that the Jacobi constant, C , for an extended spacecraft, is given by

$$C = \omega^2(x^2 + y^2) - 2\Phi_1 + \frac{Q^{jk}}{m}\partial_j g_{k,1} - 2\Phi_2 + \frac{Q^{jk}}{m}\partial_j g_{k,2} - (\dot{x}^2 + \dot{y}^2),$$

where Φ_1 and Φ_2 are the scalar potentials for each mass as given by equation (2.18).

Then, taking the time derivative of C for an extended spacecraft, we see that C only changes when Q^{ij} changes:

$$\begin{aligned}\dot{C} &= \omega^2 (2x\dot{x} + 2y\dot{y}) - 2\partial_t\Phi_1 + \frac{\dot{Q}^{jk}}{m}\partial_j g_{k,1} + \frac{Q^{jk}}{m}\partial_t\partial_j g_{k,1} \\ &\quad - 2\partial_t\Phi_2 + \frac{\dot{Q}^{jk}}{m}\partial_j g_{k,2} + \frac{Q^{jk}}{m}\partial_t\partial_j g_{k,2} - 2\dot{x}\ddot{x} - 2\dot{y}\ddot{y}, \\ &= \frac{\dot{Q}^{jk}}{m}\partial_j g_{k,1} + \frac{\dot{Q}^{jk}}{m}\partial_j g_{k,2}.\end{aligned}$$

The derivatives with respect to time vanish as the field is static and using the equations of motion, from equation (2.28), we see that the Jacobi constant only changes when Q^{jk} changes. If we again assume that these changes in Q^{jk} are discrete, the changes in the Jacobi constant are given by

$$\delta C = 3 \left(\frac{GM_1}{r_1^3} \hat{z}_{i,1} \left(\frac{\delta Q^{ij}}{m} \hat{z}_{j,1} \right) + \frac{GM_2}{r_2^3} \hat{z}_{i,2} \left(\frac{\delta Q^{ij}}{m} \hat{z}_{j,2} \right) \right) \quad (2.32)$$

which clearly shows that for a point particle, the Jacobi constant is conserved but allowing for changes in shape to an extended spacecraft, the Jacobi ‘constant’ is in general, not constant.

2.2.4 Lagrange points

Having derived equations of motion, (2.30) for the planar, circularly restricted 3-body problem, there exist a number of equilibrium points and these are the Lagrange points. At the Lagrange points, the forces acting on a pointlike test particle cancel out, allowing for it to remain at this equilibrium point. This means that in the rotating frame, for the forces in equation (2.30) to cancel out at the Lagrange points, this requires

$$\frac{\partial U}{\partial x} = \frac{\partial U}{\partial y} = 0. \quad (2.33)$$

Therefore, finding the equilibrium points requires finding extrema of the effective potential [28].

There can exist five Lagrange points in the restricted 3-body problem. The first three Lagrange points, L_1, L_2, L_3 , exist along the axis of the primary

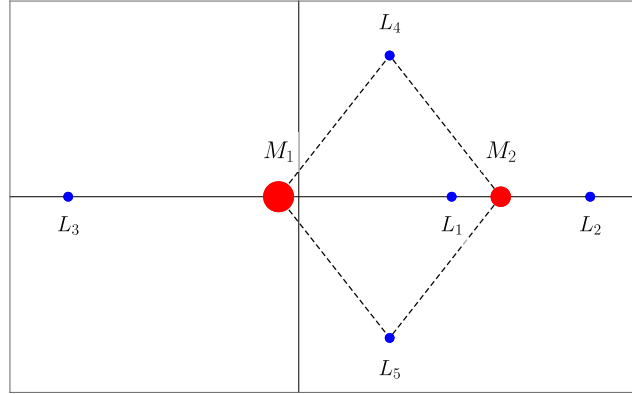


Figure 2.3: Equilibrium points for the restricted 3-body problem. The primary bodies, shown in red, are labelled as M_1 and M_2 , where the mass of M_1 is ten times greater than M_2 . The Lagrange points, shown in blue, are labelled L_1 to L_5 , with the collinear points shown along the x -axis and the equilateral points are at the apex of equilateral triangles, shown in black dashed lines, with the two primary bodies at their vertices.

bodies, which is chosen to be the x -axis. These are known as the collinear Lagrange points. The final two Lagrange points, L_4, L_5 exist at the apex of equilateral triangles with the two primary bodies at their vertices. These are known as the equilateral Lagrange points. These five points along with the positions of the two primary bodies can be seen in figure 2.3.

When looking at equilibrium points, it is common to study the motion of a pointlike particle near the Lagrange points. To start, we write perturbations from equilibrium as

$$x = x_0 + \delta x, \quad y = y_0 + \delta y,$$

where (x_0, y_0) is the location of the equilibrium point and $\delta x, \delta y$ are perturbations from equilibrium. The effective potential can then be Taylor expanded about the equilibrium point and keeping terms up to 2^{nd} order which yields

$$\begin{aligned} U &= U_0 + U_x \delta x + U_y \delta y + \frac{1}{2} U_{xx} (\delta x)^2 + U_{xy} (\delta x \delta y) + \frac{1}{2} U_{yy} (\delta y)^2, \\ &= U_0 + \frac{1}{2} U_{xx} (\delta x)^2 + U_{xy} (\delta x \delta y) + \frac{1}{2} U_{yy} (\delta y)^2, \end{aligned} \quad (2.34)$$

where U_0 is the effective potential evaluated at the equilibrium point. U_x, U_{xx}

etc. are the derivatives of the potential, evaluated at the equilibrium point and by definition, $U_x = U_y = 0$ at a Lagrange point. Using this Taylor expanded potential and substituting it into equation (2.30), the linearised equations of motion for small perturbations about an equilibrium point become

$$\begin{aligned}\delta\ddot{x} - 2\omega\delta\dot{y} &= U_{xx}\delta x U_{xy}\delta y, \\ \delta\ddot{y} + 2\omega\delta\dot{x} &= U_{xy}\delta x U_{yy}\delta y.\end{aligned}\tag{2.35}$$

We can then write the linearised equations of motion in the first order form

$$\dot{\mathbf{x}} = \mathbf{A}\mathbf{x},$$

where

$$\mathbf{x} = \begin{pmatrix} \delta x \\ \delta y \\ \delta\dot{x} \\ \delta\dot{y} \end{pmatrix}, \quad \mathbf{A} = \begin{pmatrix} 0 & 0 & 1 & 0 \\ 0 & 0 & 0 & 1 \\ -U_{xx} & -U_{xy} & 0 & 2\omega \\ -U_{xy} & -U_{yy} & -2\omega & 0 \end{pmatrix}.$$

The stability of the Lagrange points is determined by the nature of the eigenvalues of the matrix \mathbf{A} . The characteristic polynomial is

$$\begin{aligned}|\mathbf{A} - \lambda\mathbf{I}| &= 0, \\ \lambda^4 + (4\omega^2 - U_{xx} - U_{yy})\lambda^2 + U_{xx}U_{yy} - U_{xy}^2 &= 0.\end{aligned}$$

Defining a matrix \mathbf{B} such that

$$\mathbf{B} = \begin{pmatrix} U_{xx} & U_{xy} \\ U_{xy} & U_{yy} \end{pmatrix},$$

we can use the trace and determinant of \mathbf{B} to rewrite the characteristic polynomial as

$$\lambda^4 + (4\omega^2 - \text{tr}(\mathbf{B}))\lambda^2 + \det(\mathbf{B}) = 0.\tag{2.36}$$

Now solving this equation, the four eigenvalues, λ are written in terms of the trace and determinant of \mathbf{B} , we get

$$\lambda = \pm \frac{\sqrt{\text{tr}(\mathbf{B}) - 4\omega^2 \pm \sqrt{16\omega^2 - 8\omega^2 \text{tr}(\mathbf{B}) - 4\det(\mathbf{B}) + (\text{tr}(\mathbf{B}))^2}}}{\sqrt{2}}.\tag{2.37}$$

The stability of the five Lagrange points can be found by evaluating the derivatives of the potential at each equilibrium position. It can be shown that at the collinear Lagrange points

$$\begin{aligned} L_1 : U_{xx} &= -9\omega^2, & U_{yy} &= 3\omega^2, & U_{xy} &= U_{yx} = 0, \\ L_2 : U_{xx} &= +9\omega^2, & U_{yy} &= -3\omega^2, & U_{xy} &= U_{yx} = 0, \\ L_3 : U_{xx} &= -3\omega^2, & U_{yy} &= \frac{7M_2}{8M_1}\omega^2, & U_{xy} &= U_{yx} = 0. \end{aligned}$$

Using (2.37) and the derivatives of the potential, there exists two real and two purely imaginary eigenvalues, such that $\Re(\lambda) = 0$, and so, the collinear Lagrange points are saddle points and generic perturbations from the equilibrium point will result in the particle falling away [33].

Then for $L_{4,5}$, the derivatives of the potential are given by

$$\begin{aligned} L_{4,5} : U_{xx} &= \frac{3}{4}\omega^2, & U_{yy} &= \frac{9}{4}\omega^2, \\ U_{xy} &= U_{yx} = \frac{3\sqrt{3}}{4} \left(\frac{M_1 - M_2}{M_1 + M_2} \right) \omega^2. \end{aligned}$$

Substituting these in to the characteristic polynomial shows that for $L_{4,5}$ to be stable,

$$M_1 \geq 25M_2 \left(\frac{1 + \sqrt{1 - 4/625}}{2} \right).$$

So for $L_{4,5}$, if the masses of the primary bodies satisfies this condition, then there exists four, purely imaginary eigenvalues which means the Lagrange points $L_{4,5}$ will be centres allowing a point particle to orbit in the region about the equilibrium point [34].

2.2.5 Hill region

For some value of the Jacobi constant, C , we can calculate the curve in space for which the velocity in equation (2.31) goes to zero, such that $C = 2U$. These curves are called the zero velocity curves and form the boundary of the Hill regions which is the region of possible motion for a particle with Jacobi

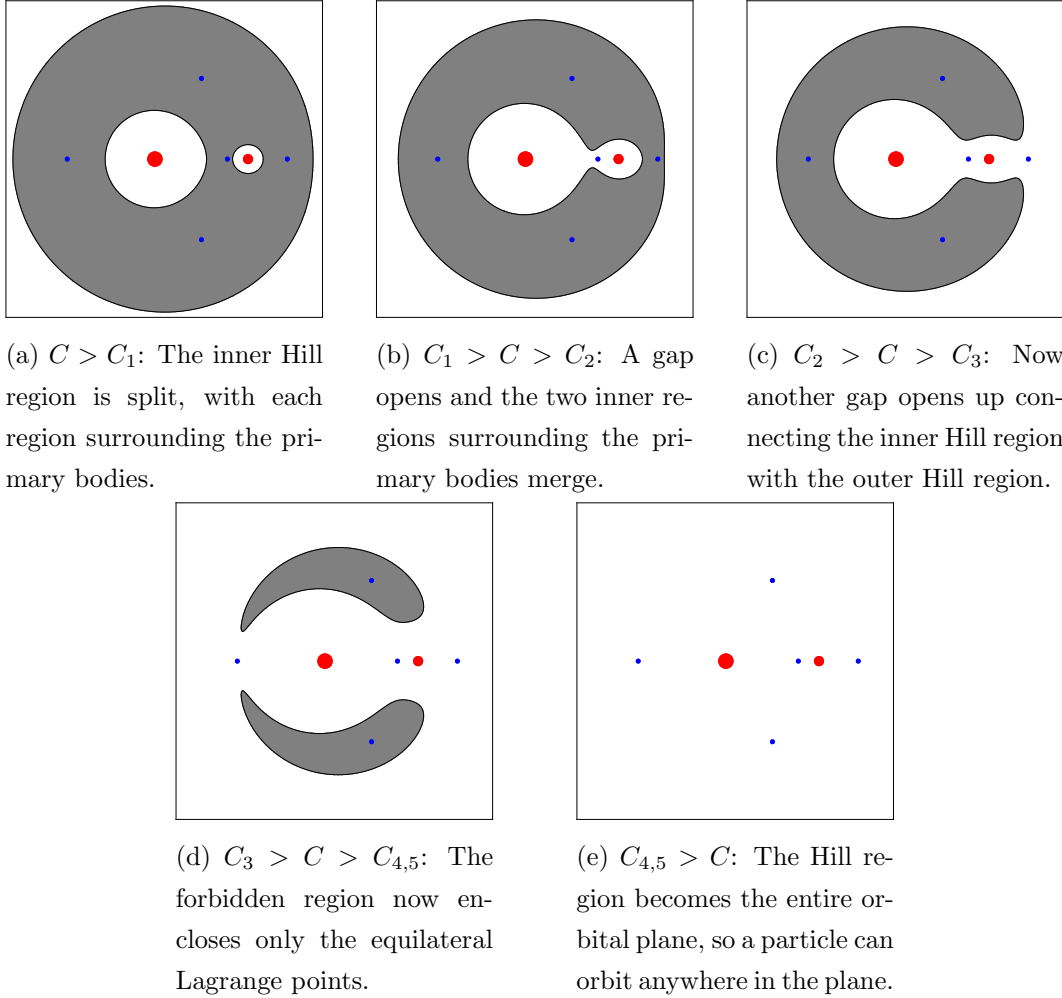


Figure 2.4: Hill regions corresponding to five different values of C . The primary bodies are shown in red and the five Lagrange points are shown in blue.

constant C [35]. The Hill regions shape depends on the value of C and the five different Hill regions are shown in figure 2.4.

In figure 2.4, the particle can only move in the white region and subsequently cannot orbit within the grey region as it is impossible to pass through the zero velocity curve. The five values of C_i are found by evaluating the Jacobi constant for a particle sitting at Lagrange point L_i and have values such that $C_1 > C_2 > C_3 > C_{4,5}$. For example, C_1 is the Jacobi constant for a particle sitting at Lagrange point 1. The value of C is also the same when evaluated at L_4 and L_5 so $C_4 = C_5 = C_{4,5}$.

As seen in figure 2.4a, the inner Hill region is split in two and as such, a particle or spacecraft with Jacobi constant $C > C_1$ which is initially in orbit about one of the primary bodies, can never orbit about the second primary body without decreasing C . When a spacecrafts Jacobi constant is such that $C_1 > C > C_2$, the two inner Hill regions merge, opening up a gap at Lagrange point 1 as seen in figure 2.4b, which allows for the spacecraft to transfer its orbit between primary bodies. Then as seen in figure 2.4c, when $C_2 > C > C_3$, another gap opens up at Lagrange point 2, which allows for the inner and outer Hill regions to merge, meaning a spacecraft can pass through this gap to the outer Hill region [36].

Chapter 3

Results

The problem of the motion of an extended spacecraft is discussed in the context of the 2-body problem first and then in the 3-body problem. In the 3-body problem, an extended spacecraft is used to perform some orbital manoeuvres and in stabilising its orbit in the region about an unstable point.

3.1 2-body problem

3.1.1 Torque-free extended spacecraft

As mentioned in section 1.2, research in to extended spacecraft adopt a barbell model while the torque exerted on the spacecraft is controlled using reaction wheels [13, 14] or by allowing the angular momentum to be transferred between the spin and orbital angular momentum [10, 12]. Even a small change in the orbital angular momentum will lead to a large spin up of the spacecraft, which could lead to it tearing itself apart. This can be seen by considering a barbell spacecraft in an initially circular orbit using the strategy described in [12]. The spacecraft raises its orbit slightly to a new circular orbit with radius $r + \Delta r$ and the centripetal acceleration of the two point masses due to the rotation would

be of order $2|\mathbf{g}|(r/\ell)^3(\Delta r/r)^2$ when the spacecraft is at its maximum length, ℓ . Even a 1% increase in radius in low Earth orbit will result in accelerations of order $(5 \times 10^5 \text{m/s}^2)(10\text{km}/\ell)^3$ [37]. It is clear then that even a small transfer of orbital angular momentum to spin angular momentum is not feasible.

Here, we instead choose to keep the spin angular momentum constant. To do this, it can be seen that for the torque, which is given by (2.21), to vanish such that $\boldsymbol{\tau} = 0$, then $Q^{ij}\hat{z}_j$ must be equal to αz^i . Therefore, we can use the eigenvector condition

$$Q^{ij}\hat{z}_j = q\hat{z}^i, \quad (3.1)$$

for some q which is an eigenvalue of the quadrupole moment associated with the eigenvector, the radial vector \hat{z}_j . This can be seen from

$$\begin{aligned} \tau_i &= -\frac{3GM}{r^3}\epsilon_{ijk}\hat{z}^j(q\hat{z}^k), \\ &= -\frac{3GM}{r^3}q\epsilon_{ijk}\hat{z}^j\hat{z}^k, \\ &= -\frac{3GM}{r^3}q(\hat{\mathbf{z}} \times \hat{\mathbf{z}})_i = 0. \end{aligned} \quad (3.2)$$

This is important in the design of any spacecraft; recalling that the torque is the rate of change of the extended spacecrafts spin angular momentum, any non-zero torque which is maintained and in the same direction for long enough, will result in the spacecraft spinning up, eventually leading to the spacecraft tearing itself apart. The eigenvalue, q can be time dependent and its sign is unconstrained. Examples of some extended spacecraft which can change the magnitude and/or sign of this eigenvalue will be discussed later in this section.

Similarly, we can now express the gravitational force exerted on an extended spacecraft in terms of this new parameter. Starting with equation

(2.20) and using the eigenvector condition, the force can now be written as

$$\begin{aligned}
F_i &= mg_i + \frac{3GM}{r^4} \left(q\hat{z}_i - \frac{5}{2} ((Q^{jk}\hat{z}_j)\hat{z}_k) \hat{z}_i \right), \\
&= mg_i + \frac{3GM}{r^4} \left(q\hat{z}_i - \frac{5}{2} q\hat{z}^k\hat{z}_k\hat{z}_i \right), \\
&= mg_i + \frac{3GM}{r^4} \left(q\hat{z}_i - \frac{5}{2} q\hat{z}_i \right), \\
&= mg_i - \frac{9}{2} \left(\frac{q}{mr^2} \right) \left(-\frac{GMm}{r^2} \right) \hat{z}_i.
\end{aligned}$$

It can be seen that the product of the term in the second bracket and the unit radial vector is just mg_i and as such we can now write the force as

$$F_i = mg_i \left(1 + \frac{9}{2} \left(\frac{q}{mr^2} \right) \right). \quad (3.3)$$

Having derived expressions for the force, torque and discrete change in energy in sections 2.1.1 to 2.1.3, we can also use the eigenvector condition to express the change in energy in terms of q . Starting with equation (2.19) and using the fact that the dot product of a unit vector with itself is one, the change in energy is

$$\delta E = -\frac{3GM}{2r^3} \delta q. \quad (3.4)$$

It can be seen from this that to gain a large change in energy, changes in q should be made when the orbital radius of the extended spacecraft is small. This is due to the the larger gradient in the gravitational field at small radii. Recalling equation (2.15) and using the discrete changes in energy, the energy can be written in terms of discrete changes in q as

$$E = E_{\text{pt}} - \frac{3GM}{2r^3} \delta q. \quad (3.5)$$

3.1.2 Changing energy and eccentricity

The gravitational field, \mathbf{g} is spherically symmetric and therefore the total angular momentum is conserved. We defined q in such a way so as to ensure $\boldsymbol{\tau} = 0$ and subsequently, the spin angular momentum of the spacecraft is constant.

This results in the orbital angular momentum, \mathbf{L} , being necessarily conserved meaning that any changes in q cannot result in any changes in \mathbf{L} . In the 2-body problem, for any elliptic orbit with eccentricity, e and semi-major axis, a , the magnitude of the orbital angular momentum is given by

$$|\mathbf{L}| = L = m\sqrt{GMa(1 - e^2)}. \quad (3.6)$$

If L is to remain constant for a torque-free spacecraft, we cannot make any changes to the semi-major axis without changing the eccentricity. Also, assuming that any changes in q are instantaneous, the energy changes when q changes. Changing q changes the potential energy and so using equation (3.5) allows U to be written in terms of q as

$$\begin{aligned} U &= m\Phi - \frac{GM}{r} \left(\frac{3}{2} \frac{q}{r^2} \right), \\ &= m\Phi + \left(-\frac{GMm}{r} \right) \left(\frac{3}{2} \frac{q}{mr^2} \right), \\ &= m\Phi \left(1 + \frac{3}{2} \frac{q}{mr^2} \right). \end{aligned} \quad (3.7)$$

Then, as a result of the conservation of angular momentum, the angular component of the kinetic energy can allow the energy from equation (2.15), to be written in terms of the effective potential energy, U_{eff} :

$$\begin{aligned} E &= \frac{1}{2}m\dot{r}^2 + \frac{L^2}{2mr^2} + U, \\ &= \frac{1}{2}m\dot{r}^2 + \frac{L^2}{2mr^2} + m\Phi \left(1 + \frac{3}{2} \frac{q}{mr^2} \right), \\ &= \frac{1}{2}m\dot{r}^2 + U_{\text{eff}}. \end{aligned} \quad (3.8)$$

$$U_{\text{eff}} = \frac{L^2}{2mr^2} - \frac{GMm}{r} \left(1 + \frac{3}{2} \left(\frac{q}{mr^2} \right) \right). \quad (3.9)$$

If the energy of an extended spacecraft is negative and the goal is to increase this energy, then the change in energy can be maximised by increasing q when r is small and decreasing it back to its original value when r is large. If this process is repeated over multiple orbits the energy will increase, all

without the use of a rocket. If the energy is increased, then it can be seen from the expressions for a and e ,

$$a = -\frac{GMm}{2E}, \quad e = \sqrt{1 - \frac{\left(\frac{L}{m}\right)^2}{GMa}}, \quad (3.10)$$

that a and therefore e must also increase. We can design a spacecraft which can switch between two different values of q such that $q = q_+$ or $q = q_-$, where $q_+ > q_-$. This means the effective potential energy, and therefore the total orbital energy, of the spacecraft can take two different values, depending on the value of q ,

$$E = E_{\text{pt}} - \frac{3GM}{2r^3}q \quad (3.11)$$

and an overall increase in energy can be achieved by setting $q = q_-$ at the spacecrafts pericentre and at apocentre, $q = q_+$. This cycle is shown in figure 3.1 and repeating this cycle allows the spacecraft to “climb up” the two effective potential energy curves for the two values of q . This strategy is outlined as follows:

1. Orbit to pericentre, set $q = q_-$.
2. Orbit to apocentre, set $q = q_+$.

The change in energy due to one cycle can be seen as ΔE in figure 3.1, where Δ is used to indicate a change in some parameter from the beginning of one cycle to the next, or from pericentre to pericentre. From equation (3.11), this means that $\Delta E = \Delta E_{\text{pt}}$ as at the beginning of each cycle, q will be the same. We start by considering the change in the effective potential energy when q switches from q_+ to q_- , using equation (3.4),

$$U_{\text{eff}}(q_+) - U_{\text{eff}}(q_-) = \delta E = -\frac{3GM}{2r^3}(q_+ - q_-). \quad (3.12)$$

Then, to calculate the change in energy over one cycle, ΔE , we use the radii of the pericentre and apocentre, given by $r_p = a(1 - e)$ and $r_a = a(1 + e)$,

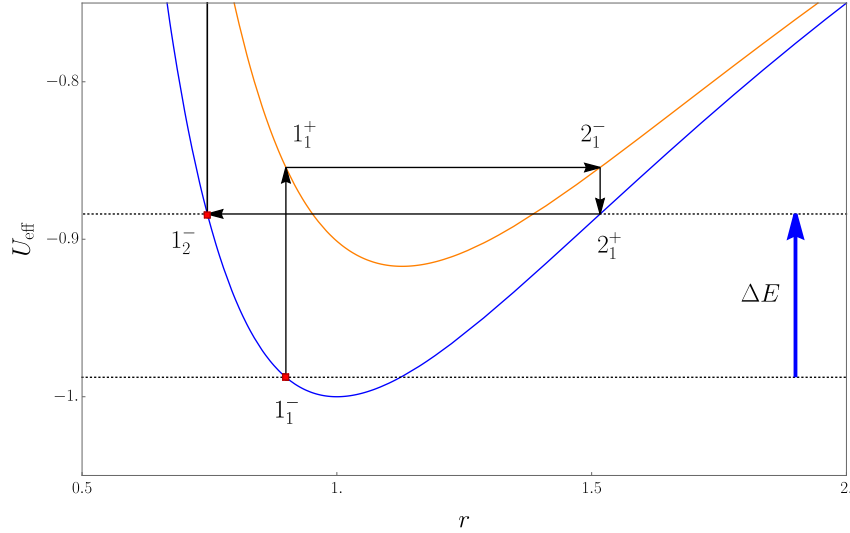


Figure 3.1: Effective potential energy curves for two values of q ; the blue curve represents $U_{\text{eff}}(q_+)$ and the orange curve represents $U_{\text{eff}}(q_-)$. The black lines indicate the cycle of switching q between q_- and q_+ . The cycle begins just before pericentre with $q = q_+$ with energy given by the lower black, dashed line. When the spacecraft reaches the pericentre, the spacecraft switches to $q = q_-$ and this switch is labelled by the points 1_1^- and 1_1^+ . The spacecraft then orbits from pericentre to apocentre, where it switches back to $q = q_+$ and this is labelled by points 2_1^- and 2_1^+ . The spacecraft then orbits back to pericentre, thus completing one cycle of switching q . The beginning and end of this cycle is indicated using red squares. The next cycle is not included but the start of which is labelled 1_2^- . The overall change in energy from the first cycle is shown by ΔE [37].

where a and e are given by equation (3.10):

$$\begin{aligned}\Delta E &= -\frac{3}{2} \frac{GMm}{a(1+e)} \left(\frac{q_+ - q_-}{ma^2(1+e)^2} \right) + \frac{3}{2} \frac{GMm}{a(1-e)} \left(\frac{q_+ - q_-}{ma^2(1-e)^2} \right), \\ &= 3 \frac{GMm}{2a} \left(\frac{q_+ - q_-}{ma^2} \right) \left(-\frac{1}{(1+e)^3} + \frac{1}{(1-e)^3} \right), \\ &= 6e \frac{GMm}{2a} \left(\frac{q_+ - q_-}{ma^2} \right) \left(\frac{3+e^2}{(1-e^2)^3} \right),\end{aligned}$$

We can then non-dimensionalise the change in energy over one cycle by dividing both sides by the absolute value of the energy, given by equation (3.8), to see the fractional change in energy per orbit, which gives

$$\frac{\Delta E}{|E|} = 6e \left(\frac{q_+ - q_-}{ma^2} \right) \left(\frac{3+e^2}{(1-e^2)^3} \right). \quad (3.13)$$

The term $(q_+ - q_-)/ma^2$ is of order $(\ell/a)^2 \ll 1$, where ℓ is the characteristic size and so, changes in a and e are small over one cycle. We can see that for fixed semi-major axis, a , the fractional change in energy increases as the orbit of the spacecraft becomes more eccentric.

We can now show that the fractional change in the semi-major axis is equal to the fractional change in the energy. This can be done by differentiating the expression for a given in equation (3.10) with respect to E ,

$$\begin{aligned}\frac{\Delta a}{\Delta E} &= \frac{d}{dE} \left(-\frac{GMm}{2E} \right) = \frac{GMm}{2E^2}, \\ &= -\frac{GMm}{2E} \frac{\Delta E}{|E|}, \\ \frac{\Delta a}{a} &= \frac{\Delta E}{|E|} = 6e \left(\frac{q_+ - q_-}{ma^2} \right) \left(\frac{3+e^2}{(1-e^2)^3} \right).\end{aligned}$$

Finally, we can derive the change in eccentricity over one cycle, this time differentiating the expression for e given in equation (3.10) with respect

to a ;

$$\begin{aligned}
\frac{\Delta e}{\Delta a} &= \frac{d}{da} \left(1 - \frac{\left(\frac{L}{m}\right)^2}{GMa} \right)^{\frac{1}{2}}, \\
\Delta e &= \frac{\Delta a}{2} \left(\frac{\left(\frac{L}{m}\right)^2}{GMa^2} \right) \left(1 - \frac{\left(\frac{L}{m}\right)^2}{GMa} \right)^{-\frac{1}{2}}, \\
&= \frac{\Delta a}{a} \frac{(1 - e^2)}{2e} = 6e \left(\frac{q_+ - q_-}{ma^2} \right) \left(\frac{3 + e^2}{(1 - e^2)^3} \right) \frac{1 - e^2}{2e}, \\
&= 3 \left(\frac{q_+ - q_-}{ma^2} \right) \left(\frac{3 + e^2}{(1 - e^2)^2} \right).
\end{aligned} \tag{3.14}$$

It can be seen from equations (3.13) and (3.14) that as expected from the stronger tidal gradients on orbits with smaller pericentres, this strategy of increasing the energy is most effective at high eccentricities for fixed a .

If the strategy of switching q is repeated N times, the total change in eccentricity can be found by applying equation (3.14) for each of the N cycles. We can then say that the eccentricity of the spacecrafts orbit is a function of N such that $e = e(N)$. As changes in q are discrete, the eccentricity also changes in discrete steps so this function for e is difficult to find in a simple form, although it can be approximated by using the differential equation formed by replacing Δe with de/dN and allow N to have non-integer values.

$$\Delta e \Rightarrow \frac{de}{dN} = 3 \left(\frac{q_+ - q_-}{ma^2} \right) \left(\frac{3 + e^2}{(1 - e^2)^2} \right) \tag{3.15}$$

Using the conservation of L and defining the characteristic number of cycles, N_{char} such that

$$N_{\text{char}}^{-1} \equiv \frac{3\sqrt{3}}{(1 - e_0^2)^2} \left(\frac{q_+ - q_-}{ma_0^2} \right), \tag{3.16}$$

where a_0 and e_0 are the semi-major axis and eccentricity of the spacecrafts initial orbit, the solution to the differential equation (3.15) is given by

$$e = \sqrt{3} \tan \left(\frac{N}{N_{\text{char}}} + \tan^{-1} \left(\frac{e_0}{\sqrt{3}} \right) \right). \tag{3.17}$$

This solution to the differential equation is plotted in figure 3.2, as well as the eccentricity found by numerically solving the equations of motion.

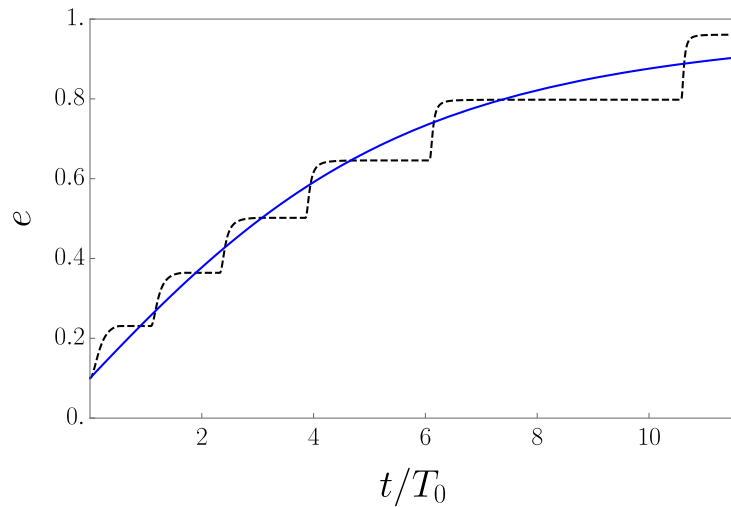


Figure 3.2: Increase in eccentricity using the strategy of switching q . The solid blue line is the plot of equation (3.17) along with using $dt/dN = 2\pi a^{\frac{3}{2}}/\sqrt{GM}$ to convert the function from one depending on N to one depending on t . The dashed black line is found by directly numerically integrating the equations of motion, equation (2.28), using tolerances that are automatically chosen for *NDSolve* in *Mathematica*. The integration method is also automatically chosen for what *Mathematica* believes to be the best method. The initial orbital period is T_0 , $e_0 = 1/10$, $q = q_+ = 0$ and $q = q_- = -ma_0^2/100$ [37].

Starting with this expression, we can then also find the semi-major axis and energy as a function of N by using the equations introduced in (3.10). This results in deriving the following

$$a = \frac{a_0(1 - e_0)^2}{1 - 3 \tan \left(\frac{N}{N_{\text{char}}} + \tan^{-1} \left(\frac{e_0}{\sqrt{3}} \right) \right)^2}, \quad (3.18)$$

$$E = \frac{E_0 \left(1 - 3 \tan \left(\frac{N}{N_{\text{char}}} + \tan^{-1} \left(\frac{e_0}{\sqrt{3}} \right) \right)^2 \right)}{(1 - e_0)^2}, \quad (3.19)$$

where E_0 is the initial energy of the spacecraft. These results can be used to calculate the number of orbits needed to change between any two values of a or E_{pt} . Equation (3.17) can be used to calculate the number of cycles needed to change between two eccentricities and can be used to find the number of cycles needed to escape the primary body. For an orbit to be one which allows the spacecraft to escape, the final eccentricity must satisfy $e_f \geq 1$. As such, we set the left hand side of equation (3.17) equal to one and solve to get

$$1 = \sqrt{3} \tan \left(\frac{N}{N_{\text{char}}} + \tan^{-1} \left(\frac{e_0}{\sqrt{3}} \right) \right), \quad (3.20)$$

$$N_{\text{esc}} = \left(\frac{\pi}{6} - \tan^{-1} \left(\frac{e_0}{\sqrt{3}} \right) \right) N_{\text{char}}.$$

The process describing switching q to increase the energy of the spacecraft also increases a and e , as mentioned before. However, it can be seen by plotting the pericentre, $r_p = a(1 - e)$, as a function of N , as shown in figure 3.3, that it decreases over time. As such, a spacecraft looking to escape the primary body in the number of cycles given in equation (3.20), would likely crash in to the primary body before escaping. An example of the orbits of a spacecraft using this strategy is shown in figure 3.4, where the precession of the orbit can clearly be seen due to the perturbative force introduced from the extended body effects.

Alternatively, step 1 and 2 from above could be changed such that now the spacecraft

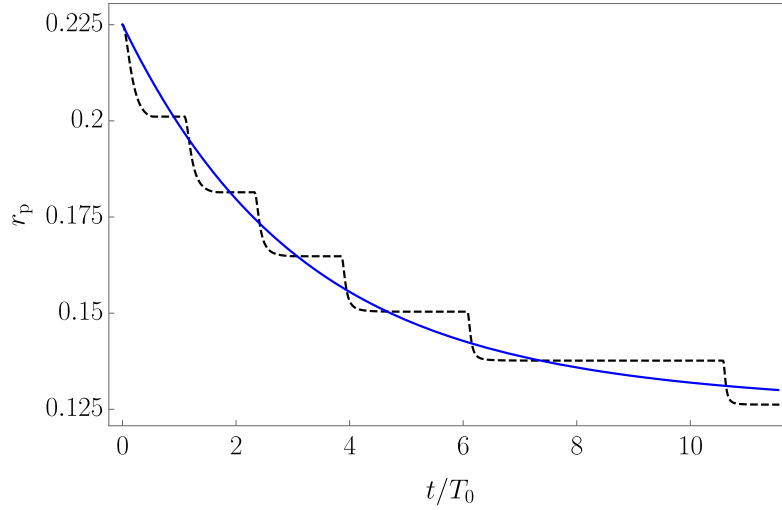


Figure 3.3: Decrease in pericentre using cyclic changes in q to increase energy. The solid blue line is the plot of the pericentre, again with using $dt/dN = 2\pi a^{3/2}/\sqrt{GM}$ to convert the function to be dependent on t . The dashed black line was found using the same method of directly numerically integrating the equations of motion, as in figure 3.2. T_0 , e_0 and q_{\pm} are the same as in figure 3.2.

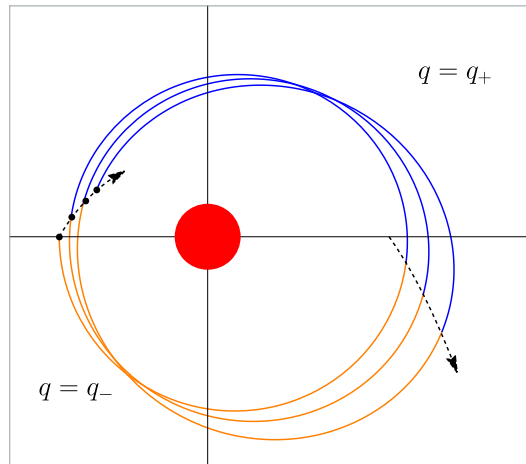


Figure 3.4: Numerical solutions for the orbits of an extended spacecraft using the eccentricity increasing strategy. In the part of the orbit shown in orange, $q = q_-$ and in the blue portion, $q = q_+$. The extended spacecraft orbits counter-clockwise and begins at the black dot. The precession of the orbit due to the increasing eccentricity strategy can be seen from the dashed black lines showing the precession of the pericentre and apocentre, with the black points representing the instantaneous pericentres. Once again, the values for e_0 and q_{\pm} are the same as in figure 3.2.

1. Orbits to pericentre, set $q = q_+$.
2. Orbits to apocentre, set $q = q_-$.

This strategy would instead result in a decrease in energy and therefore a decrease in the semi-major axis and eccentricity. The conservation of L in this strategy would mean the orbit of the extended spacecraft would become less eccentric and would eventually become circular, where no more changes could be made due to there being no distinction between the pericentre/apocentre. In this strategy, equation (3.17) is still the solution to the differential equation when we replace $N_{\text{char}} \rightarrow -N_{\text{char}}$. The number of cycles needed to get to the final circular orbit is found by setting the left hand side of equation (3.17) to be equal to zero, which can then be solved to get

$$\begin{aligned}
0 &= \sqrt{3} \tan \left(\frac{N}{-N_{\text{char}}} + \tan^{-1} \left(\frac{e_0}{\sqrt{3}} \right) \right), \\
N_{\text{circ}} &= N_{\text{char}} \tan^{-1} \left(\frac{e_0}{\sqrt{3}} \right).
\end{aligned} \tag{3.21}$$

3.1.3 Controlling the precession

It has been shown that a spacecraft using extended body effects can control its energy, its semi-major axis and its orbital eccentricity, although it cannot control them independently. However, it can also control its orbital precession, this time independently of controlling the eccentricity. For $q = 0$, the orbit will not precess so the orbital orientation is fixed, as shown in section 2.1.4. When the eigenvalue is non-zero, the force exerted on the spacecraft no longer satisfies (2.22) and so the orientation of an elliptic orbit rotates. To measure this rotation, we use the LRL vector as given by (2.23) and this rotation can be described using the angular velocity, $\boldsymbol{\omega}$.

If the LRL vector for an orbit is given by \mathbf{A}_1 and after a spacecrafts orbit precesses, the LRL vector pointing towards the new instantaneous pericentre is \mathbf{A}_2 . The difference between these two is given by

$$\mathbf{A}_2 = \mathbf{A}_1 + \Delta \mathbf{A} = \mathbf{A}_1 + \dot{\mathbf{A}} \Delta t.$$

Then taking the cross product of this with \mathbf{A}_1 and using the fact that the angle between \mathbf{A}_1 and \mathbf{A}_2 is given by $\theta = |\omega|\Delta t$, we get

$$|\mathbf{A} \times (\mathbf{A} + \dot{\mathbf{A}}\Delta t)| = |\mathbf{A}||\mathbf{A} + \dot{\mathbf{A}}\Delta t| \sin \theta.$$

Then using the small angle approximation and the fact that the magnitude of the LRL vector is the instantaneous eccentricity, we can write

$$\begin{aligned} |(\mathbf{A} \times \dot{\mathbf{A}})\Delta t| &= e^2(|\omega|\Delta t), \\ |\omega| &= \frac{|\mathbf{A} \times \dot{\mathbf{A}}|}{e^2}. \end{aligned}$$

The vector $\mathbf{A} \times \dot{\mathbf{A}}$ points out of the plane, meaning that ω will point out of the plane and so, the precession will occur in the orbital plane. We can then write

$$\boldsymbol{\omega} = \frac{\mathbf{A} \times \dot{\mathbf{A}}}{e^2}.$$

Using equation (2.23), we can evaluate this expression for a torque-free spacecraft which has a force given by (3.3) exerted on it. First, taking the time derivative of (2.23) while using $\ddot{\mathbf{z}} = \mathbf{F}/m$ and $\dot{r} = \dot{\mathbf{z}} \cdot \mathbf{z}/r$, we get

$$\dot{\mathbf{A}} = \frac{\mathbf{F} \times \mathbf{L}}{GMm^2} + \frac{\mathbf{z}}{r^2} \left(\frac{\dot{\mathbf{z}} \cdot \mathbf{z}}{r} \right) - \frac{\dot{\mathbf{z}}}{r}.$$

We can write the angular momentum as $\mathbf{L} = m\mathbf{z} \times \dot{\mathbf{z}}$ and using this and expanding the force given in equation (3.3), we can substitute these in to the equation derived above, such that $\dot{\mathbf{A}}$ can be written as

$$\dot{\mathbf{A}} = \frac{9}{2} \left(\frac{q}{mr^2} \right) (\mathbf{g} \times \mathbf{L}). \quad (3.22)$$

From this, we can see that if $q = 0$, then \mathbf{A} is conserved.

To evaluate the angular velocity, ω , having found $\dot{\mathbf{A}}$ in equation (3.22), we then take the cross product of it with \mathbf{A} from equation (2.23), using the triple product $\mathbf{a} \times (\mathbf{b} \times \mathbf{c}) = (\mathbf{a} \cdot \mathbf{c})\mathbf{b} - (\mathbf{a} \cdot \mathbf{b})\mathbf{c}$, giving

$$\begin{aligned} \mathbf{A} \times \dot{\mathbf{A}} &= \frac{9}{2} \left(\frac{q}{mr^2} \right) \left(\frac{\dot{\mathbf{z}} \times \mathbf{L}}{GMm} - \frac{\mathbf{z}}{r} \right) \times (\mathbf{g} \times \mathbf{L}), \\ &= \frac{9}{2} \left(\frac{q}{mr^2} \right) \mathbf{L} \left(\frac{GMm}{r} (|\dot{\mathbf{z}}|^2 - \dot{r}^2) - \frac{9}{2mr^2} \right). \end{aligned}$$

The true anomaly, ν , is the angle of the spacecraft away from its pericentre. The change in the true anomaly with respect to time is given by

$$\dot{\nu} = \frac{L}{mr^2}, \quad (3.23)$$

and the term $|\dot{\mathbf{z}}|^2 - \dot{r}^2$ is just the square of $\dot{\nu}$, times the radius squared. Using this, we can write the cross product of \mathbf{A} and $\dot{\mathbf{A}}$ as

$$\mathbf{A} \times \dot{\mathbf{A}} = \frac{9}{2} \left(\frac{q}{mr^2} \right) \mathbf{L} \left(\frac{r\dot{\nu}^2}{GMm} - \frac{1}{mr^2} \right).$$

Using the expression for the magnitude of the angular momentum given in equation (3.10) together with

$$r = \frac{\left(\frac{L}{m}\right)^2}{GM(1 + e \cos \nu)} = \frac{a_0(1 - e_0^2)}{1 + e \cos \nu}, \quad (3.24)$$

we now divide the cross product of $\mathbf{A} \times \dot{\mathbf{A}}$ by the eccentricity squared to find the angular velocity to be

$$\begin{aligned} \boldsymbol{\omega} &= \frac{\mathbf{A} \times \dot{\mathbf{A}}}{e^2} = \frac{q}{mr^2} \left(\frac{9\mathbf{L}}{2emr^2} \right) \left(\frac{r^3\dot{\nu}^2}{GM_e} - \frac{1}{e} \right), \\ &= \frac{q}{mr^2} \left(\frac{9\mathbf{L}}{2emr^2} \right) \cos \nu. \end{aligned} \quad (3.25)$$

So a torque-free spacecraft with force given by (3.3) exerted on it precesses at an instantaneous rate given by (3.25). Letting ψ be the total precession angle such that $\boldsymbol{\omega} = \dot{\psi} \hat{\mathbf{L}}$, we can integrate both sides of this to calculate the precession angle per orbit, $\Delta\psi$. We can use the fact that $\Delta\psi = \int \dot{\psi} dt = \int |\boldsymbol{\omega}| dt$. Then, the right hand side of the integral must be written as integral with respect to ν which can be done using equation (3.23). The integral can then be written as

$$\Delta\psi = \frac{9}{2me} \int \frac{q}{r^2} \cos \nu d\nu.$$

We will then use equation (3.24) and integrate ν between 0 and 2π , where $q = +q_+$ for $0 < \nu < \pi$ and $q = q_-$ for $\pi < \nu < 2\pi$, and this choice for

switching q is the same as the choice made when increasing the eccentricity, as used earlier in section 3.1.2. We can write $\Delta\psi$ in terms of the sum of two integrals

$$\begin{aligned}\Delta\psi &= \frac{9}{2me} \int_0^{2\pi} \frac{q(1 + e \cos \nu)^2}{a_0^2(1 - e_0^2)} \cos \nu d\nu, \\ &= \frac{9}{2mea_0^2(1 - e_0^2)^2} \\ &\quad \left(q_+ \int_0^\pi (1 + e \cos \nu)^2 \cos \nu d\nu + q_- \int_\pi^{2\pi} (1 + e \cos \nu)^2 \cos \nu d\nu \right).\end{aligned}$$

Then evaluating the integrals, the precession angle per orbit is given by

$$\Delta\psi = \frac{9\pi}{2(1 - e_0^2)^2} \left(\frac{q_+ + q_-}{ma_0^2} \right). \quad (3.26)$$

It can be seen here that the precession angle per orbit is determined by the sum of the eigenvalues, $q_+ + q_-$ whereas the change in eccentricity per orbit, as given by equation (3.14), is determined by the difference between the eigenvalues, $q_+ - q_-$. This allows a torque-free spacecraft to independently vary the eccentricity and precession for appropriate choice of q_+ and q_- . The precession angle per orbit is also constant and so the total precession angle after N orbits is $\psi = N\Delta\psi$.

As the change in eccentricity depends on the difference in eigenvalues and the change in precession depends on the sum, we can use the eccentricity increasing strategy while choosing the eigenvalues such that the sum is zero. This means the orbit of the extended spacecraft will not precess but the eccentricity will still increase and an example of non-precessing but eccentricity increasing orbits is shown in figure 3.5.

3.1.4 Example extended spacecraft

Having defined the time-dependent control parameter, q , it can be shown how the design of an extended spacecraft can be used to allow the sign and magnitude of q to change by changing the shape of the spacecraft. In general, for

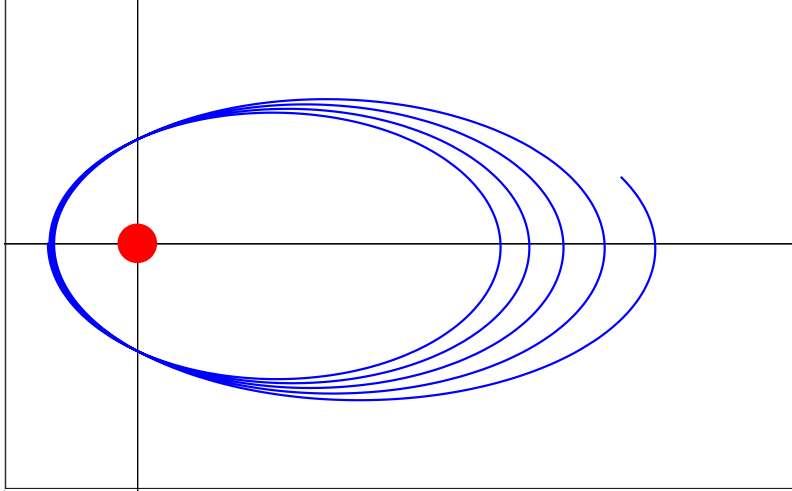


Figure 3.5: Non-precessing orbits of spacecraft with $q = q_+ = (0.02)^2/24$ and $q = q_- = -(0.02)^2/24$. This results in $q_+ + q_- = 0$ and so from equation (3.26), the orbits do not precess while the eccentricity still increases.

the purpose of this research, no specific model for the spacecraft was used but here, we explore two examples of an extended spacecraft.

To begin, we can think of an extended spacecraft, shaped like a barbell, with total mass m , which has two equal, spherically symmetric masses, separated by some length ℓ . The density of each of the point masses is given by

$$\rho = c\delta(x)\delta(y)\delta\left(z - \frac{\ell}{2}\right) + c\delta(x)\delta(y)\delta\left(z + \frac{\ell}{2}\right),$$

$$\int \rho d^3\mathbf{x} = 2c = m,$$

where X, Y, Z are the coordinates of the point masses such that $(X, Y, Z) = (0, 0, \pm\frac{\ell}{2})$, $\delta(a - A)$ is the Dirac Delta Function and c is some constant to be calculated. Evaluating the triple integral in the density, c is found to be equal to $m/2$ for this barbell shaped spacecraft. As each point mass is equal, we can

now write the quadrupole moment as

$$\begin{aligned}
Q_{ij} &= \int \int \int \rho \left(d_i d_j - \frac{1}{3} \delta^{ij} \text{tr}(Q_{ij}) \right) dx dy dz, \\
&= \frac{m}{2} \int \int \int \delta(x - X) \delta(y - Y) \delta(z - Z) \\
&\quad \left(d_i d_j - \frac{1}{3} \delta^{ij} \text{tr}(Q_{ij}) \right) dx dy dz + 2^{nd} \text{mass}, \\
&= m \int \int \int \delta(x - X) \delta(y - Y) \delta(z - Z) \\
&\quad \left(d_i d_j - \frac{1}{3} \delta^{ij} \text{tr}(Q_{ij}) \right) dx dy dz,
\end{aligned}$$

with $d_i = (x - z)_i$ and where third line incorporates both masses. Using the position of each point mass relative to the centre of mass position we can write $d_1 = d_2 = 0$ and $d_3 = \pm \ell/2$. Once again, the integrals can be evaluated and the quadrupole moment can be written in matrix form as

$$\begin{aligned}
Q_{ij} &= m \left(\begin{pmatrix} 0 & 0 & 0 \\ 0 & 0 & 0 \\ 0 & 0 & \frac{\ell^2}{4} \end{pmatrix} - \frac{1}{3} \begin{pmatrix} \frac{\ell^2}{4} & 0 & 0 \\ 0 & \frac{\ell^2}{4} & 0 \\ 0 & 0 & \frac{\ell^2}{4} \end{pmatrix} \right), \\
&= \begin{pmatrix} -\frac{m\ell^2}{12} & 0 & 0 \\ 0 & -\frac{m\ell^2}{12} & 0 \\ 0 & 0 & \frac{m\ell^2}{6} \end{pmatrix}, \tag{3.27}
\end{aligned}$$

which shows the eigenvalues of Q_{ij} as the diagonal components, corresponding to the three orthogonal, unit, coordinate vectors which are the three eigenvectors. Two of the eigenvalues are degenerate meaning the two corresponding eigenvectors do not have to be orthogonal to one another but must be orthogonal to the third, non-degenerate eigenvector. From this, if we align the spacecraft to be perpendicular to the orbital plane, the two degenerate eigenvectors will exist in the orbital plane and therefore, the radial vector can be an eigenvector of the quadrupole moment allowing the spacecraft to be torque-free.

Using this example of a barbell shaped spacecraft, the magnitude of the degenerate eigenvalue $q = -m\ell^2/12$ associated with the radial eigenvector \hat{z}_i can be varied by changing the distance ℓ between the point masses.

In the case of a barbell extended spacecraft, the degenerate eigenvalue, $q = -m\ell^2/12$ is always negative or equal to zero, or $q \leq 0$, and so only the magnitude of the eigenvalue can be changed, not the sign. With a different configuration for the extended spacecraft, it can also be shown using the same arguments that the sign of q can also be varied along with the magnitude. Instead of two point masses, we now use the example of two equal mass hoops of radius R separated by a distance ℓ . In this example, we can convert to cylindrical coordinates and the density of each hoop can be written as

$$\rho = c\delta(r - R)\delta(z - Z),$$

$$\int \rho d^3\mathbf{x} = c \int \int \int r\delta(r - R)\delta(z - Z)d\theta dr dz = \frac{m}{2}.$$

First evaluating the integral with respect to θ and then again, evaluating the other two integrals, we can calculate the value of c to be

$$\begin{aligned} \frac{m}{2} &= 2\pi c \int \int r\delta(r - R)\delta(z - Z)dr dz, \\ &= 2\pi R c \int \delta(z - Z)dz, \\ &= 2\pi R c, \\ c &= \frac{m}{2} \frac{1}{2\pi R}. \end{aligned}$$

Using this value for c , we can now write the quadrupole moment in terms of the density for the two hoops, where both hoops have equal mass

$$\begin{aligned} Q_{ij} &= \int \int \int \rho \left(d_i d_j - \frac{1}{3} \delta^{ij} \text{tr}(Q_{ij}) \right) d\theta dr dz, \\ &= \frac{m}{2} \frac{1}{2\pi R} \int \int \int r\delta(r - R)\delta(z - Z) \\ &\quad \left(d_i d_j - \frac{1}{3} \delta^{ij} \text{tr}(Q_{ij}) \right) d\theta dr dz + 2^{nd} \text{hoop}, \\ &= \frac{m}{2\pi R} \int \int \int r\delta(r - R)\delta(z - Z) \\ &\quad \left(d_i d_j - \frac{1}{3} \delta^{ij} \text{tr}(Q_{ij}) \right) d\theta dr dz, \end{aligned}$$

where the third line incorporates both hoops. Again, $d_i = (x - z)_i$ and now in cylindrical coordinates, the position of any point on one of the hoops is $(r \cos \theta, r \sin \theta, \pm \ell/2)$, meaning $d_1 = r \cos \theta$, $d_2 = r \sin \theta$ and $d_3 = \pm \ell/2$. Now, once again evaluating the integrals, rewriting the quadrupole moment in matrix form

$$\begin{aligned}
Q_{ij} &= \frac{m}{2\pi R} \int \int \int \delta(r - R) \delta(z - Z) \\
&\quad \left(\begin{pmatrix} r^3 \cos^2 \theta & r^3 \cos \theta \sin \theta & r^2 \cos \theta \frac{\ell}{2} \\ r^3 \cos \theta \sin \theta & r^3 \sin^2 \theta & r^2 \sin \theta \frac{\ell}{2} \\ r^2 \cos \theta \frac{\ell}{2} & r^2 \sin \theta \frac{\ell}{2} & r \frac{\ell^2}{4} \end{pmatrix} - \frac{1}{3} \delta^{ij} \text{tr}(Q_{ij}) \right) dr dz d\theta, \\
&= \frac{m}{2\pi R} \int \\
&\quad \left(\begin{pmatrix} R^3 \cos^2 \theta & R^3 \cos \theta \sin \theta & R^2 \cos \theta \frac{\ell}{2} \\ R^3 \cos \theta \sin \theta & R^3 \sin^2 \theta & R^2 \sin \theta \frac{\ell}{2} \\ R^2 \cos \theta \frac{\ell}{2} & R^2 \sin \theta \frac{\ell}{2} & R \frac{\ell^2}{4} \end{pmatrix} - \frac{1}{3} \delta^{ij} \text{tr}(Q_{ij}) \right) d\theta, \\
&= \frac{m}{2\pi R} \left(\begin{pmatrix} \pi R^3 & 0 & 0 \\ 0 & \pi R^3 & 0 \\ 0 & 0 & 2\pi R \frac{\ell^2}{4} \end{pmatrix} - \frac{1}{3} \delta^{ij} \text{tr}(Q_{ij}) \right), \\
&= \begin{pmatrix} \frac{mR^2}{2} & 0 & 0 \\ 0 & \frac{mR^2}{2} & 0 \\ 0 & 0 & \frac{m\ell^2}{4} \end{pmatrix} - \begin{pmatrix} \frac{mR^2}{3} + \frac{m\ell^2}{12} & 0 & 0 \\ 0 & \frac{mR^2}{3} + \frac{m\ell^2}{12} & 0 \\ 0 & 0 & \frac{mR^2}{3} + \frac{m\ell^2}{12} \end{pmatrix}, \\
&= \begin{pmatrix} \frac{mR^2}{6} - \frac{m\ell^2}{12} & 0 & 0 \\ 0 & \frac{mR^2}{6} - \frac{m\ell^2}{12} & 0 \\ 0 & 0 & -\frac{mR^2}{3} + \frac{m\ell^2}{6} \end{pmatrix}.
\end{aligned} \tag{3.28}$$

Similar to the example of a barbell spacecraft with two point masses, there exists two degenerate eigenvalues associated with two eigenvectors. Here, to ensure the spacecraft is torque-free, we again choose to align the craft such that the radial vector is an eigenvector of the quadrupole moment. Now the magnitude and the sign of q can be changed by varying ℓ . The critical value

of ℓ needed to change the sign of q is given by

$$\begin{aligned}\frac{mR^2}{6} &= \frac{m\ell^2}{12} \\ \ell &= \sqrt{2}R.\end{aligned}\tag{3.29}$$

It can also be seen that the first example extended spacecraft with two point masses is a limiting case for the two hoops example. This can be seen in the limit as $R \rightarrow 0$, the eigenvalues reduce to that of the eigenvalues found in the example of a barbell shaped spacecraft.

3.1.5 Numerical examples

At this point, we have shown analytically that an extended spacecraft can use extended body effects to change its orbital energy, eccentricity and precession by following a strategy for switching q . Now we ask the question of the time frames involved in changing these parameters. In section 3.1.2, equation (3.17) describes the eccentricity as a function of the number of orbits about the primary body and in figure 3.2, this function is shown to be in agreement with solution obtained from directly numerically integrating the equations of motion.

Here, we will give an example of the number of orbits required to escape an orbit, and the total precession angles involved when performing this manoeuvre. We also adopt the model most commonly used in the literature [10–15], the barbell shaped spacecraft. The initial eccentricity of the orbit is $e_0 = 0.1$ and we will consider a spacecraft starting in a low Earth orbit, with $a_0 = 6.8 \times 10^6 m$. We set the eigenvalues as $q = q_+ = 0$ and $q = q_- = -m\ell^2/12$, where $\ell = a_0/10 = 6.8 \times 10^5 m$.

Using these values and equations (3.20) and (3.21), we can calculate the number of orbits needed for the spacecraft to escape and the total precession angle of the orbit due to extended body effects. The mass of the spacecraft is irrelevant as q is always proportional to m and so, the mass will always cancel in these calculations. In this problem, changing the value of q between

q_+ and q_- involves changing the length, ℓ of the barbell between $\ell = 0m$ and $\ell = 6.8 \times 10^5m$.

The number of orbits needed for the extended spacecraft to escape is $N_{esc} \approx 879$ and multiplying this by precession angle per orbit, the total precession angle is $\psi = N_{esc}\Delta\psi \approx -1.3\text{rad}$.

Alternatively, a spacecraft with the same parameters as above but now it wishes to circularise its orbit can do so by following the decreasing eccentricity strategy, set $N_{char} \rightarrow -N_{char}$ and use equation (3.21) to find that $N_{circ} \approx 109$ and the total precession angle in this case is $\psi \approx -0.2\text{rad}$. In these cases, the total precession angle being negative tells us the direction of the precession is opposite to the direction of motion of the spacecraft, as seen in figure 3.4.

A spacecraft with a length of $680km$ may cause some engineering issues so a spacecraft with a shorter length may be more “realistic”. Decreasing $q_+ - q_-$ for an extended spacecraft will increase the number of orbits needed to escape or to circularise its orbit and so in designing an extended spacecraft, some balance would need to be found.

3.2 3-body problem

Having looked at the motion of an extended spacecraft in the 2-body problem, it is now necessary to develop this idea and look at it in the 3-body problem. Much like in the 2-body problem, where we can use an extended spacecraft to change its orbit, we can do the same in the 3-body problem. However, in the 3-body problem, with the introduction of a second primary body, there are more possibilities of what can be achieved using extended body effects to change a spacecrafts orbit.

3.2.1 Gravitational force and torque

As in the 2-body problem where the torque, force and change in energy all depend on the quadrupole moment only via $Q^{ij}\hat{z}_j$ and as such, the eigenvector condition, (3.1), could be used to derive expressions to now depend on a single parameter, q . The use of the eigenvector condition is made possible by aligning the spacecraft such that the radial vector, \hat{z}_j is an eigenvector of Q^{ij} .

However, in the 3-body problem, the gravitational force, torque and the change in the Jacobi constant, depend on $Q^{ij}\hat{z}_{j,1}$ and $Q^{ij}\hat{z}_{j,2}$ simultaneously. In this case, if we now wish for the total torque to vanish then $Q^{ij}\hat{z}_{j,1} = \alpha\hat{z}_1^i$ and $Q^{ij}\hat{z}_{j,2} = \alpha\hat{z}_2^i$ and therefore, $Q^{ij}\hat{z}_{j,1} = q\hat{z}_1^i$ and $Q^{ij}\hat{z}_{j,2} = q\hat{z}_2^i$, for some q . As we require that the torque from both primary bodies vanishes, both radial vectors for the two primary bodies must be eigenvectors of Q^{ij} .

So aligning the spacecraft such that the two radial vectors for both primary bodies are eigenvectors of Q^{ij} allows the spacecraft to be torque-free. As shown in section 3.1.4, there will exist two degenerate eigenvalues, q which are associated with two degenerate eigenvectors. The two degenerate eigenvectors do not need to be perpendicular to one another but must be perpendicular to the third eigenvector. This means that the two radial vectors can simultaneously be eigenvectors, with the eigenvalue associated with these eigenvectors being the degenerate eigenvalues. Using the example of a barbell shaped extended spacecraft, the degenerate eigenvalue associated with the two radial unit vectors would be $q = -ml^2/12$.

Starting with the gravitational torque, for equation (2.25) to vanish, the two radial unit vectors must be eigenvectors:

$$\boldsymbol{\tau}_{\text{tot}} = -\frac{3GM_1}{r_1^3}q(\mathbf{z}_1 \times \mathbf{z}_1)_i - \frac{3GM_2}{r_2^3}q(\mathbf{z}_2 \times \mathbf{z}_2)_i = 0. \quad (3.30)$$

This again means the extended spacecraft is torque-free even in the 3-body problem.

Having shown this, the gravitational force exerted on an extended space-

craft by the two primary bodies can be written as the sum of the force used in the 2-body problem for both primary bodies

$$F_{i,\text{tot}} = mg_{i,1} \left(1 + \frac{9}{2} \frac{q}{mr_1^2} \right) + mg_{i,2} \left(1 + \frac{9}{2} \frac{q}{mr_2^2} \right). \quad (3.31)$$

We can then split this expression into its \hat{x} and \hat{y} components and use these in the expression for the total force on a spacecraft in a rotating frame, as derived in equation (2.28). The equations of motion in the rotating frame when extended body effects are included are written as

$$\begin{aligned} m\ddot{x} &= -\frac{GM_1m}{r_1^2} \left(1 + \frac{9}{2} \frac{q}{mr_1^2} \right) \frac{x-x_1}{r_1} - \frac{GM_2m}{r_2^2} \left(1 + \frac{9}{2} \frac{q}{mr_2^2} \right) \frac{x-x_2}{r_2} \\ &\quad + 2m\omega\dot{y} + m\omega^2x, \\ m\ddot{y} &= -\frac{GM_1m}{r_1^2} \left(1 + \frac{9}{2} \frac{q}{mr_1^2} \right) \frac{y-y_1}{r_1} - \frac{GM_2m}{r_2^2} \left(1 + \frac{9}{2} \frac{q}{mr_2^2} \right) \frac{y-y_2}{r_2} \\ &\quad - 2m\omega\dot{x} + m\omega^2y, \end{aligned} \quad (3.32)$$

where (x_1, y_1) and (x_2, y_2) are the fixed positions of the two primary bodies, M_1 and M_2 , in the rotating frame and we can set their positions to be along the x-axis, such that $y_1 = y_2 = 0$ and ω is the angular velocity of the rotating frame. Again, here we use x and y to represent the rotating vectors for the position of the spacecraft in the rotating frame.

3.2.2 Non-dimensionalised equations of motion

Given the equations of motion for an extended spacecraft in a rotating frame, we can now non-dimensionalise them. This is done as there are more parameters than are physically relevant (e.g. the mass of the spacecraft) in the equations of motion, given in equation (3.32). It also helps to show how the relevant parameters scale when viewed as a ratio of some characteristic quantities of the system [38].

To begin deriving the non-dimensionalised equations of motion, we must first identify the independent and dependent variables. The time, t is the only

independent variable and the x and y positions are dependent variables. Then, we can replace these variables with some quantity which is scaled by some characteristic unit of measure, which results in

$$t = \gamma t_c, \quad x = \xi l_c, \quad y = \eta l_c,$$

where γ , ξ and η are the non-dimensionalised variables for time and the two position variables, respectively. The characteristic units of measure are the characteristic time and characteristic length, which is the same for both x and y . As the radii to the spacecraft from both primary bodies depend on x and y , we can also replace them with non-dimensionalised radii, $\rho_{1,2}$, combined with the characteristic length, and the positions of the primary bodies is $\xi_1 = x_1/l_c$ and $\xi_2 = x_2/l_c$. Using these replacements, the equations of motion, equation (3.32), can be rewritten as

$$\begin{aligned} \frac{d^2\xi}{d\gamma^2} &= -\frac{GM_1 t_c^2}{\rho_1^2 l_c^3} \left(1 + \frac{9}{2} \frac{q}{\rho_1^2 m l_c^2}\right) \frac{\xi - \xi_1}{\rho_1} \\ &\quad - \frac{GM_2 t_c^2}{\rho_2^2 l_c^3} \left(1 + \frac{9}{2} \frac{q}{\rho_2^2 m l_c^2}\right) \frac{\xi - \xi_2}{\rho_2} + 2t_c\omega \frac{d\eta}{d\gamma} + t_c^2\omega^2\xi, \\ \frac{d^2\eta}{d\gamma^2} &= -\frac{GM_1 t_c^2}{\rho_1^2 l_c^3} \left(1 + \frac{9}{2} \frac{q}{\rho_1^2 m l_c^2}\right) \frac{\eta}{\rho_1} \\ &\quad - \frac{GM_2 t_c^2}{\rho_2^2 l_c^3} \left(1 + \frac{9}{2} \frac{q}{\rho_2^2 m l_c^2}\right) \frac{\eta}{\rho_2} - 2t_c\omega \frac{d\xi}{d\gamma} + t_c^2\omega^2\eta, \end{aligned}$$

where in general for some extended spacecraft, q has dimensions $[ML^2]$ and as such, the term $q/\rho^2 m l_c^2$ is unitless. We now define the characteristic units so that the coefficients of as many terms in the equations of motion go to one. We start by first noticing that coriolis and centrifugal forces are proportional to $t_c\omega$ and $(t_c\omega)^2$, respectively. Remembering that ω is the angular velocity of the frame, we can define the characteristic time such that

$$\omega = \sqrt{\frac{G(M_1 + M_2)}{(-x_1 + x_2)^3}} = \sqrt{\frac{GM_{\text{tot}}}{l_c^3}} = t_c^{-1}, \quad (3.33)$$

where M_{tot} is the sum of the masses of the primary bodies and $-x_1 + x_2$ is the distance between the two primary bodies, which we define to be the characteristic length, l_c of the system. We can also define a dimensionless

mass ratio to simplify the expressions. Defining $\mu = M_2/M_{\text{tot}}$ means we can write $1 - \mu = M_1/M_{\text{tot}}$ using the definition of the total mass. Then using the definition of the centre of mass of the two primary bodies and the characteristic length, we can write the positions of the primary bodies as $\xi_1 = -\mu$ and $\xi_2 = 1 - \mu$.

Using the definition of μ , the characteristic units and the positions ξ_1 and ξ_2 , we can write the non-dimensionalised equations of motion for a spacecraft in a rotating frame as

$$\begin{aligned}\frac{d^2\xi}{d\gamma^2} &= -\frac{1-\mu}{\rho_1^2} \left(1 + \frac{9}{2} \frac{q}{m\rho_1^2 l_c^2}\right) \frac{\xi + \mu}{\rho_1} \\ &\quad - \frac{\mu}{\rho_2^2} \left(1 + \frac{9}{2} \frac{q}{m\rho_2^2 l_c^2}\right) \frac{\xi - 1 + \mu}{\rho_2} + 2\frac{d\eta}{d\gamma} + \xi, \\ \frac{d^2\eta}{d\gamma^2} &= -\frac{1-\mu}{\rho_1^2} \left(1 + \frac{9}{2} \frac{q}{m\rho_1^2 l_c^2}\right) \frac{\eta}{\rho_1} \\ &\quad - \frac{\mu}{\rho_2^2} \left(1 + \frac{9}{2} \frac{q}{m\rho_2^2 l_c^2}\right) \frac{\eta}{\rho_2} - 2\frac{d\xi}{d\gamma} + \eta.\end{aligned}$$

In these equations, we have used a number of symbols to represent non-dimensionalised variables. However, for convenience and familiarity, from this point on, the equations will be written such that the normal symbols for dimensionful variables, such as t , x , y and r will be used to represent their non-dimensionalised quantities, again, in the rotating frame. This means the non-dimensionalised equations of motion can be written in terms of these familiar symbols, which results in

$$\begin{aligned}\ddot{x} &= -\frac{1-\mu}{r_1^2} \left(1 + \frac{9}{2} \frac{q}{r_1^2}\right) \frac{x + \mu}{r_1} - \frac{\mu}{r_2^2} \left(1 + \frac{9}{2} \frac{q}{r_2^2}\right) \frac{x - 1 + \mu}{r_2} + 2\dot{y} + x, \\ \ddot{y} &= -\frac{1-\mu}{r_1^2} \left(1 + \frac{9}{2} \frac{q}{r_1^2}\right) \frac{y}{r_1} - \frac{\mu}{r_2^2} \left(1 + \frac{9}{2} \frac{q}{r_2^2}\right) \frac{y}{r_2} - 2\dot{x} + y,\end{aligned}\tag{3.34}$$

where q also represents the non-dimensionalised eigenvalue.

3.2.3 Change in Jacobi constant

Having shown an extended spacecraft can be torque-free in the 3-body problem, starting with equation (2.31) and using the non-dimensionalised equations of motion, the potential U is given by

$$U = \frac{1}{2}(x^2 + y^2) + \frac{1-\mu}{r_1} \left(1 + \frac{3}{2} \frac{q}{r_1^2}\right) + \frac{\mu}{r_2} \left(1 + \frac{3}{2} \frac{q}{r_2^2}\right), \quad (3.35)$$

and therefore, the Jacobi constant in terms of q is

$$\begin{aligned} C &= 2U - \dot{x}^2 - \dot{y}^2, \\ &= 2 \left(\frac{1}{2}(x^2 + y^2) + \frac{1-\mu}{r_1} \left(1 + \frac{3}{2} \frac{q}{r_1^2}\right) + \frac{\mu}{r_2} \left(1 + \frac{3}{2} \frac{q}{r_2^2}\right) \right) - \dot{x}^2 - \dot{y}^2, \quad (3.36) \\ &= x^2 + y^2 + 2 \left(\frac{1-\mu}{r_1} \left(1 + \frac{3}{2} \frac{q}{r_1^2}\right) + \frac{\mu}{r_2} \left(1 + \frac{3}{2} \frac{q}{r_2^2}\right) \right) - \dot{x}^2 - \dot{y}^2. \end{aligned}$$

Starting with equation (2.32) and for a torque-free spacecraft in non-dimensionalised system, the change in Jacobi constant due to switching q is proportional to the change in eigenvalue,

$$\delta C = 3\delta q \left(\frac{1-\mu}{r_1^3} + \frac{\mu}{r_2^3} \right). \quad (3.37)$$

Again, similar to the 2-body problem, to gain a large change in C , q should change when the orbital radius is small. This is somewhat more straight forward in the 2-body problem as the spacecrafts orbit will have a clear near and far point, per cycle. However, in the 3-body problem, the spacecraft has two orbital radii, one for each primary body and as such, it can be more difficult to decide when to change q . To overcome this, we can instead take the time derivative of equation (3.37) to find when the change in C is at a minimum and maximum:

$$\delta \dot{C} = -9\delta q \left(\frac{1-\mu}{r_1^4} \dot{r}_1 + \frac{\mu}{r_2^4} \dot{r}_2 \right). \quad (3.38)$$

When this changes sign, the change in C is at a minimum or maximum and it is at these radii that C should be changed to gain the largest change in

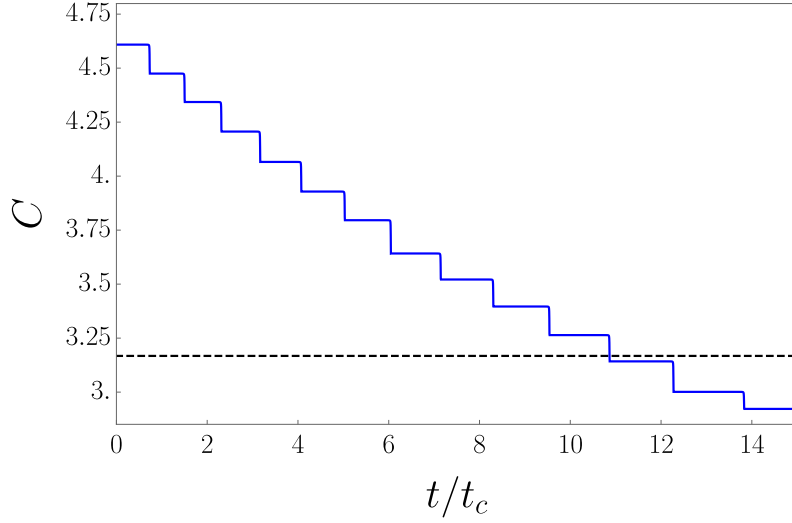


Figure 3.6: Decrease in C using the strategy of switching q whenever $\delta\dot{C} = 0$. The extended spacecraft orbits in the gravitational field of the two primary bodies and changes q such that the Jacobi constant is decreased over time. The black dashed line is given by $C = C_1$. The x -axis is non-dimensionalised time where t_c is the inverse of the angular velocity of the frame, given by equation (3.33).

C . If the goal of this extended spacecraft is to decrease the Jacobi constant over time as it orbits in the 3-body problem, then we can use a strategy similar to that used in the 3-body problem. We can once again design a spacecraft which can change q between q_- and q_+ , such that $q_+ > q_-$. To decrease the Jacobi constant, the following strategy is used:

q changes whenever $\delta\dot{C} = 0$ and the value of q after this change is given by

1. $\delta\ddot{C} < 0$, set $q = q_-$.
2. $\delta\ddot{C} > 0$, set $q = q_+$.

As seen in figure 3.6, an extended spacecraft which adopts this strategy for changing q can decrease C over time. Like in the 2-body problem, the strategy can also be reversed so that the spacecraft systematically increases C .

As mentioned in section 2.2.5, the shape of the Hill region is given by

the value of the Jacobi constant of a spacecraft meaning that using the strategy to decrease C , we can also change the Hill region. For a spacecraft with an initial Jacobi constant, C such that $C > C_1$, as seen in figure 2.4a, it can use the strategy detailed above to decrease C to be less than C_1 . This means a gap will open up in the inner Hill region at L_1 as seen in figure 2.4b. Initially, the spacecraft could only orbit about one of the primary bodies, depending on whether it started in the inner Hill region surrounding M_1 or M_2 . Now, by changing the Jacobi constant such that $C_1 > C$, a spacecraft can now orbit about the two primary bodies.

A possible application of this strategy is for an extended spacecraft, starting with $C > C_1$ within the inner Hill region surrounding M_1 , to first decrease its Jacobi constant such that $C_1 > C$, which would result in the Hill region changing from figure 2.4a to 2.4b. The spacecraft could then pass through the gap at L_1 after which it then increases C such that $C > C_1$ only this time, the spacecraft is now within the inner Hill region surrounding M_2 and the gap at L_1 has closed. This means the Hill region changes shape from 2.4b back to 2.4a.

If the strategy of decreasing C is continued, the spacecraft can decrease C to be less than C_2 , leading to a gap to open at L_2 , allowing the spacecraft to orbit in the outer Hill region. This case is shown in figure 2.4c and would result in the spacecraft escaping from the primary bodies.

3.2.4 Orbits to decrease Jacobi constant

Having shown that it is possible for an extended spacecraft to decrease its Jacobi constant to be less than C_1 , allowing to transfer its orbit from one primary body to the other, we now ask how long this process might take. We can directly numerically integrate the non-dimensionalised equations of motion, as derived in equation (3.34), to calculate the number of orbits needed for $C = C_1$.

There are a number of free parameters used in the numerical integration; the mass ratio of the two primary bodies, μ , the minimum and maximum value of the non-dimensionalised eigenvalue, $q = q_{\pm}$, the initial Jacobi constant, C_0 with $C_0 > C_1$ and the initial radius, r_0 , from M_1 . The value of C_1 is calculated by finding the positions of the Lagrange points numerically and evaluating (3.36) with the velocity of the spacecraft equal to zero at L_1 .

As a starting point for the analysis of an extended spacecraft in the 3-body problem, the spacecrafts initial position is on the x -axis and to the left of M_1 . The initial velocity in the x direction is equal to 0 and the velocity in the y direction is calculated by rearranging the equation for the Jacobi constant given by equation (2.31) and using the negative root of \dot{y}^2 so that the spacecraft orbits counter-clockwise about M_1 . Therefore, the initial position and velocity of the extended spacecraft, with $C_0 > C_1$, used in the numerical integration of the equations of motion are

$$\begin{aligned}x_0 &= -(r_0 + \mu), \\y_0 &= 0, \\\dot{x}_0 &= 0, \\\dot{y}_0 &= -\sqrt{2U_0 - C_0},\end{aligned}\tag{3.39}$$

where U_0 is the initial value of (3.35) and depends on r_0 and μ .

In the non-dimensionalised equations of motion, (3.34), q is a piecewise constant which follows the strategy from section 3.2.3 and is therefore a function of non-dimensionalised time. The shape of the Hill region with these initial conditions is dependent on C_0 and μ and so by solving for a point along the x -axis for which $2U = C_0$, we find the maximum initial value for x_0 , which we call x_{\max} . Therefore the maximum possible initial radius from M_1 is given by $r_{\max} = -(x_{\max} + \mu)$. This maximum initial position as well as the range of possible initial positions for a spacecraft, for some example Hill region with $C > C_1$, is shown in figure 3.7.

The Jacobi constant as given by equation (3.36), is a function of non-dimensionalised time, $C(t)$ as the position and velocity of the spacecraft are

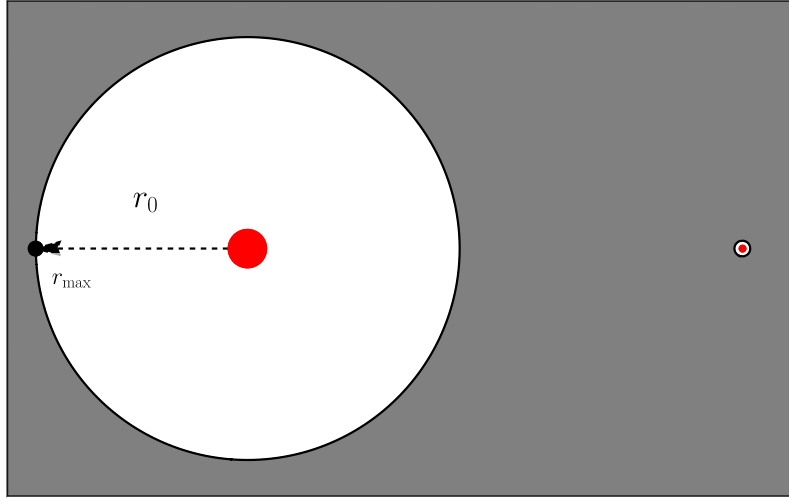


Figure 3.7: Maximum initial position given by the black point with the range of possible values for r_0 , where r_0 is in the range $(0, r_{\max})$, is shown as the black dashed arrow. The Hill region for this system is also shown.

dependent on time. The equations of motion were integrated with respect to time so by solving $C(t) = C_1$ for some time, t_1 , we can find the time needed for the Jacobi constant to decrease to C_1 . This was done by directly numerically integrating the equations of motion, equation (3.34), using an automatically chosen integration method for *NDSolve* in *Mathematica*.

We now want to find the number of orbits the extended spacecraft completes about M_1 for $t < t_1$. In the Kepler problem, an orbit can be thought of as a repeating trajectory around a primary body. However, in cases where an orbit is precessing, such as an extended body in the 3-body problem, the orbit will not repeat and so we will need to consider two definitions for a precessing orbit. The first of these definitions is to say that one orbit is the trajectory between the two consecutive points at which the spacecraft is at its closest approach to a primary body. This definition of an orbit will be referred to as an instantaneous orbit. The second definition for a precessing orbit used in this work is the trajectory for which the spacecraft orbits through 2π radians and this will be called an angular orbit.

First looking at the number of instantaneous orbits, in the decreasing

C strategy, q switches whenever $\delta\dot{C} = 0$, where $\delta\dot{C}$ is given by (3.38). This means q switches at each instantaneous pericentre and apocentre, or twice per instantaneous orbit. So the number of instantaneous orbits, N_{inst} , to decrease C to C_1 can be found by dividing the number of times $\delta\dot{C} = 0$ by two.

Then looking at the number of angular orbits, as the spacecraft is initially on the x -axis with $y_0 = 0$, we can start by dividing the number of times $y(t) = 0$ by two as the spacecraft will usually¹ cross the x -axis twice per angular orbit. This gives the number of angular orbits in the rotating frame, N_{rot} . Then, the rotation of the frame must also be considered; the frame rotates $N_{\text{frame}} = t_1/T_c$ times for $t < t_1$, where $T_c = 2\pi/\omega = 2\pi$, with ω being the angular velocity of the frame which is equal to one in non-dimensionalised units. So the number of angular orbits needed to decrease the extended spacecrafts Jacobi constant to C_1 is $N_{\text{ang}} = N_{\text{rot}} + N_{\text{frame}}$.

3.2.5 Numerical results for 2-body limit

The free parameters to choose to calculate N_{inst} and N_{ang} are μ , r_0 , q_{\pm} and C_0 . It is most convenient to set the values of μ , q_{\pm} and C_0 and then use $0 < r_0 < r_{\text{max}}$ to calculate the corresponding values for N_{inst} and N_{ang} .

To begin the numerical analysis of the problem, we first look at the limiting case of the 3-body problem where $\mu \rightarrow 0$. The 3-body problem becomes a 2-body problem when we set $\mu = 0$ and so we start with this choice for μ . From this, $C_1 = 3$ and we choose $C_0 = 2C_1$. Finally, the values for the non-dimensionalised eigenvalues are chosen to be $q = q_+ = 0$ and $q = q_- = -(0.02)^2/12$. Using the chosen values of μ and C_0 , we can determine the initial shape of the Hill region and find r_{max} . Figure 3.8 shows the number of instantaneous orbits, shown in blue and the number of angular orbits, in red, needed for an extended spacecraft to decrease C to C_1 . More details of the numerical results shown in these plots will be discussed in section 3.2.9.

¹The spacecraft can in some cases cross the x -axis more than twice per angular orbit but this number is negligible when compared to the total number of angular orbits.

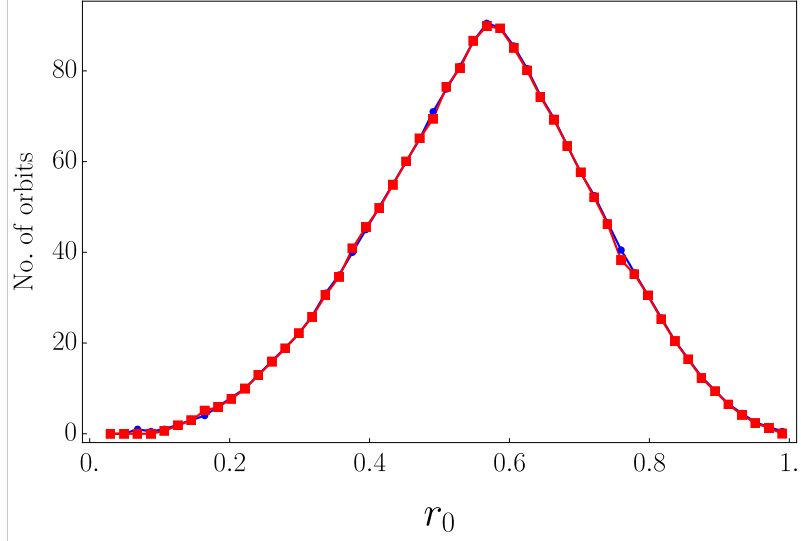


Figure 3.8: Number of orbits for $C = C_1$ with $\mu = 0$, $C_0 = 2C_1$ and eigenvalues $q = q_+ = 0$ and $q = q_- = -(0.02)^2/12$. The number of instantaneous orbits are shown in blue and the number of angular orbits are shown in red. Some details of the numerical results shown in these plots will be discussed further in section 3.2.9.

From the figure, it is clear that the number of instantaneous orbits is approximately equal to the number of angular orbits and as this is a 2-body problem, the number of orbits here should be equal to the number of orbits predicted by the results derived in the 2-body problem in section 3.1.2. In the 2-body problem, we can calculate the eccentricity of the extended spacecrafts orbit using equation (3.17) and using this, we can calculate the number of orbits needed to change the eccentricity from the initial value to some final eccentricity, e_f by

$$N = \left(\tan^{-1} \left(\frac{e_f}{\sqrt{3}} \right) - \tan^{-1} \left(\frac{e_0}{\sqrt{3}} \right) \right) N_{\text{char}}. \quad (3.40)$$

To use this result in the $\mu = 0$ case in the 3-body problem, we need to derive some expressions for e_0 and e_f using parameters used in the numerical integration of the equations of motion. We first start with e_f ; in the 3-body problem, the x coordinate of L_1 can be approximated using perturbation theory and is given by

$$L_{1,x} = R \left(1 - \left(\frac{\mu}{3} \right)^{1/3} \right), \quad (3.41)$$

in dimensionful units and to lowest order in μ [39]. In the $\mu = 0$ case, the position of L_1 becomes equal to R , the distance between the two primary bodies. This was chosen to be the characteristic length, l_c and so the x coordinate of L_1 is $R/l_c = 1$ in the non-dimensionalised system. As discussed in section 3.2.3, when $C = C_1$, the two inner Hill regions combine as a gap opens at L_1 . This also means that the Hill region opens at a distance equal to the apocentre of the spacecrafts orbit such that

$$\frac{R}{l_c} = \frac{a_f(1 + e_f)}{l_c} = 1.$$

Using this and the fact that in the 2-body problem, and therefore for $\mu = 0$, \mathbf{L} is conserved, we can express the final eccentricity as

$$\begin{aligned} L^2 &= m^2 GM a_0 (1 - e_0^2), \\ a_f(1 - e_f)(1 + e_f) &= a_0(1 - e_0)(1 + e_0), \\ R(1 - e_f) &= r_0(1 + e_0), \\ e_f &= 1 - r_0(1 + e_0), \end{aligned} \tag{3.42}$$

where we initially assume that $r_0 = a_0(1 - e_0)$. Next, the characteristic orbits, N_{char} can be expressed in terms of e_0 and r_0 using equation (3.16), such that

$$\begin{aligned} N_{\text{char}}^{-1} &= \frac{3\sqrt{3}(q_+ - q_-)}{a_0^2 ((1 - e_0)(1 + e_0))^2}, \\ &= \frac{3\sqrt{3}(q_+ - q_-)}{r_0^2 (1 + e_0)^2}. \end{aligned} \tag{3.43}$$

Finally, e_0 can be expressed in terms of C_0 and r_0 , using equation (3.36) with $q = 0$. As $\mu = 0$, the initial x coordinate of the spacecraft is just r_0 which allows C_0 to be written as

$$C_0 = r_0^2 + \frac{2}{r_0} - \dot{y}_0^2. \tag{3.44}$$

The initial velocity in the rotating frame is equal to the difference between the velocity of the spacecraft in the non-rotating frame and the velocity of the rotation of the frame. The velocity in the non-rotating frame for $\mu = 0$ will be

the *vis-viva* equation [40], which in non-dimensionalised units is

$$v_{\text{NR}} = \sqrt{\frac{1 + e_0}{r_0}},$$

where again the sign of e_0 depends on whether r_0 is the pericentre or apocentre of the initial orbit. Given that r_0 is either a pericentre or apocentre, the velocity of the rotation of the frame is

$$|\mathbf{v}_{\text{frame}}| = |\boldsymbol{\omega} \times \mathbf{x}| = |\boldsymbol{\omega}| |\mathbf{x}| = r_0.$$

As the spacecraft initially has a negative velocity in the y direction, it orbits in the same direction as the rotation of the frame so \dot{y}^2 can be expressed in terms of v_{NR} and v_{frame} as

$$\begin{aligned} \dot{y}_0^2 &= \left(\sqrt{\frac{1 + e_0}{r_0}} - r_0 \right)^2, \\ &= \frac{1}{r_0} + \frac{e_0}{r_0} + r_0^2 - 2r_0 \sqrt{\frac{1 + e_0}{r_0}}. \end{aligned}$$

Substituting this in to equation (3.44) then allows the initial Jacobi constant to be expressed in terms of e_0 and r_0 resulting in

$$\begin{aligned} C_0 &= r_0^2 + \frac{2}{r_0} - \left(\frac{1}{r_0} + \frac{e_0}{r_0} + r_0^2 - 2r_0 \sqrt{\frac{1 + e_0}{r_0}} \right), \\ &= \frac{1}{r_0} - \frac{e_0}{r_0} + 2\sqrt{\frac{r_0^2(1 + e_0)}{r_0}}, \\ &= \frac{1 - e_0}{r_0} + 2\sqrt{r_0(1 + e_0)}. \end{aligned} \tag{3.45}$$

Rearranging this yields an expression for the initial eccentricity expressed in terms of free parameters used in the numerical integration of the equations of motion:

$$e_0 = 1 - C_0 r_0 + 2r_0^3 + 2\sqrt{2r_0^3 - C_0 r_0^4 + r_0^6}. \tag{3.46}$$

For some value of C_0 , we can plot the initial eccentricity against the initial radius, $0 < r_0 < r_{\text{max}}$. In figure 3.9, we can see that at some r_0 , the

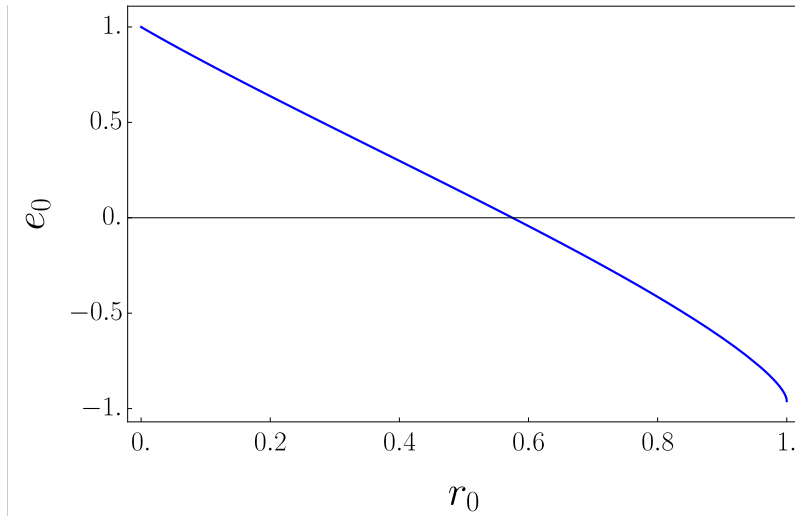


Figure 3.9: Initial eccentricity against the initial radius for $C_0 = 2C_1$.

eccentricity becomes negative. It is at this point that the initial position of the spacecraft changes from being the pericentre to the apocentre of the initial orbit. Therefore, the root of this expression gives the initial radius at which the initial orbit is circular, before any extended body or precession effects begin.

If we interpret negative eccentricities in this way the initial assumption that r_0 is the initial pericentre is not needed. When the initial eccentricity is negative, $r_0 = a_0(1 - (-e_0)) = a_0(1 + e_0)$ and so r_0 is the apocentre of the initial orbit. Having derived expressions for e_0 , e_f and N_{char} in terms of free parameters used in numerical integration, we can plot equation (3.40) against r_0 , in figure 3.10 along with the numerical data shown in figure 3.8.

To reiterate, the data presented in figure 3.10 is the number of instantaneous and angular orbits needed for an extended spacecraft to decrease its Jacobi constant to C_1 , while following the strategy outlined in section 3.2.3. The black, dashed curve represents the analytic result derived from the 2-body problem for the number of orbits between two eccentricities, which was converted to be the number of orbits between two Jacobi constants, namely decreasing from C_0 to C_1 . As the $\mu = 0$ case is just the 2-body problem, the numerical data should be in agreement with the analytic result. As can be seen from figure 3.10, this is not the case and there is some discrepancy between

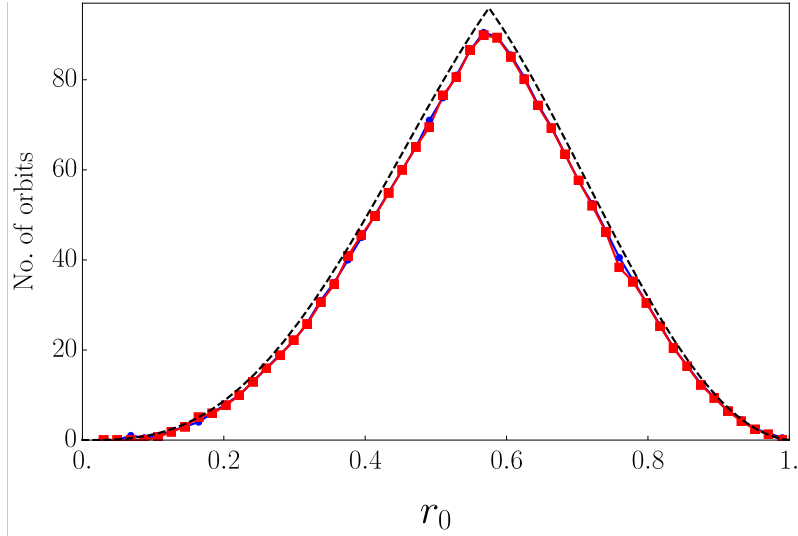


Figure 3.10: Numerical and analytic results for number of orbits to decrease $C = C_1$. The numerical results are the same as in figure 3.8 now with equation (3.40), the black dashed curve. The numerical results should be in agreement with the analytic results derived from the 2-body problem. However, this is not the case and it is unclear as to the reason behind the difference in results.

the results.

The introduction of counting of the number of angular orbits was done in an attempt to eliminate this discrepancy but clearly, it did not. The problem was then also analysed in the non-rotating frame; the forces acting on the extended spacecraft now only include the gravitational forces from the primary bodies. The Jacobi constant must also be modified as it must be consistent with the Jacobi constant in the rotating frame. In the non-dimensionalised system with $\mu = 0$, the Jacobi constant can be written as

$$C = \frac{2}{r_1} + |\mathbf{X}|^2 - |\dot{\mathbf{X}}|^2,$$

where \mathbf{X} is the position in the rotating frame and is related to the position in the non-rotating frame, \mathbf{x} , by $\mathbf{X} = R(t)\mathbf{x}$. $R(t)$ is the rotation matrix being rotated by the non-dimensionalised angle t . A property of the rotation matrix

is the fact that $|\mathbf{X}| = |\mathbf{x}|$. The rotation matrix is given by

$$R(\theta) = R(t) = \begin{pmatrix} \cos t & -\sin t \\ \sin t & \cos t \end{pmatrix}.$$

The derivative of \mathbf{X} is $\dot{\mathbf{X}} = \frac{dR}{dt}\mathbf{x} + R\dot{\mathbf{x}}$ and so the magnitude of the velocity squared is

$$\begin{aligned} |\dot{\mathbf{X}}|^2 &= \dot{\mathbf{X}}^T \dot{\mathbf{X}} = (\dot{R}\mathbf{x} + R\dot{\mathbf{x}})^T (\dot{R}\mathbf{x} + R\dot{\mathbf{x}}), \\ &= \dot{R}^T \dot{R}\mathbf{x}^T \mathbf{x} + \dot{R}^T R\mathbf{x}^T \dot{\mathbf{x}} + R^T \dot{R}\mathbf{x}^T \mathbf{x} + R^T R\dot{\mathbf{x}}^T \dot{\mathbf{x}}, \\ &= |\mathbf{x}|^2 + |\dot{\mathbf{x}}|^2 + 2R^T \dot{R}\mathbf{x}^T \mathbf{x}. \end{aligned} \quad (3.47)$$

We then need to calculate the product $R^T \dot{R}$ so we calculate the derivative and the transpose of the rotation matrix as

$$\frac{dR}{dt} = \dot{R} = - \begin{pmatrix} \sin t & \cos t \\ -\cos t & \sin t \end{pmatrix}, \quad R^T = \begin{pmatrix} \cos t & \sin t \\ -\sin t & \cos t \end{pmatrix}.$$

Using these we find that the product of the derivative and the transpose of the rotation matrix is given by

$$R^T \dot{R} = - \begin{pmatrix} \cos t & \sin t \\ -\sin t & \cos t \end{pmatrix} \begin{pmatrix} \sin t & \cos t \\ -\cos t & \sin t \end{pmatrix} = - \begin{pmatrix} 0 & 1 \\ -1 & 0 \end{pmatrix}.$$

Returning then to the Jacobi constant, we can substitute (3.47) using the product of the derivative and the transpose of the rotation matrix to get

$$\begin{aligned} C &= \frac{2}{r_1} + |\mathbf{x}|^2 - \left(|\mathbf{x}|^2 + |\dot{\mathbf{x}}|^2 - 2 \begin{pmatrix} 0 & 1 \\ -1 & 0 \end{pmatrix} \dot{\mathbf{x}}^T \mathbf{x} \right), \\ &= \frac{2}{r_1} - |\dot{\mathbf{x}}|^2 + 2(xy - \dot{x}y). \end{aligned} \quad (3.48)$$

Now using the initial conditions (3.39) and the velocity in the non-rotating frame used in deriving (3.45), we show that we get the same expression for the Jacobi constant in the non-rotating frame as was found in the rotating

frame. This can be seen from

$$\begin{aligned}
 C &= \frac{2}{r_1} - \left(\sqrt{\frac{(1+e_0)}{r_0}} \right)^2 + 2(-r_0) \left(-\sqrt{\frac{(1+e_0)}{r_0}} \right), \\
 &= \frac{1-e_0}{r_0} + 2\sqrt{r_0(1+e_0)}.
 \end{aligned}$$

As expected, we obtain the same expression for the Jacobi constant as it is independent of the rotation of the frame. As such, the discrepancy between analytical and numerical results remains when analysing the problem in the non-rotating frame.

Although the numerical and analytical results do not exactly agree, there are still some details that can be considered. The first is to look at the number of orbits as $r_0 \rightarrow 0$. As seen from equation (3.37), there is a larger change in the Jacobi constant when the radii are small. For very small and very large r_0 , the orbits are extremely eccentric, as seen from figure 3.9 and recalling from section 3.1.2 that these strategies are enhanced for larger eccentricities.

Finally, looking at the peak of the analytic number of orbits in figure 3.10, this occurs at the initial radius at which the initial orbit is circular, so $e_0 = 0$ from figure 3.9. This again can be explained by the fact that in contrast to small and large values of r_0 , smaller changes in C are possible when the eccentricity is small.

3.2.6 Numerical results for low mass ratio

Despite the disagreement between results found in section 3.2.5 it is still possible to look at cases where $\mu > 0$. As an example, using the same values for the parameters as in figure 3.8 but now with $\mu = 0.01$, the number of instantaneous and angular orbits are shown in figure 3.11.

It can be seen that the number of orbits calculated for $\mu = 0$ differ only

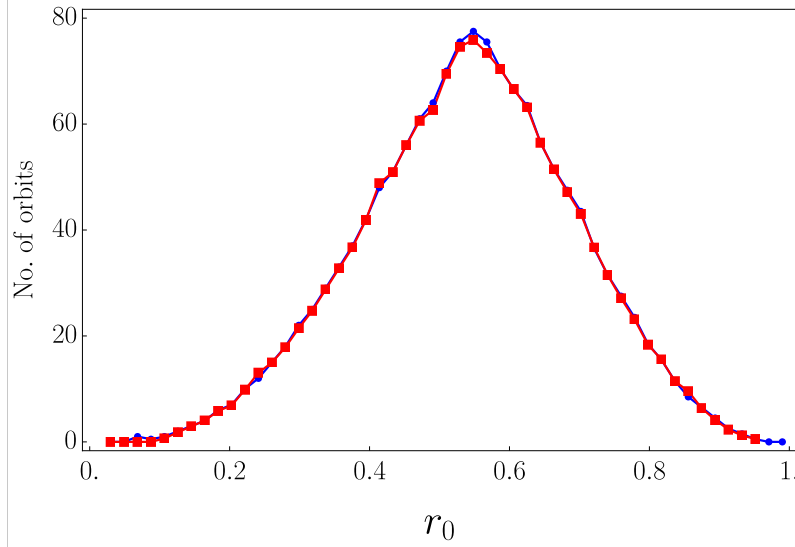


Figure 3.11: Number of orbits for $C = C_1$ with $\mu = 0.01$, $C_0 = 2C_1$ and eigenvalues $q = q_+ = 0$ and $q = q_- = -(0.02)^2/12$. The number of instantaneous orbits are shown in blue and the number of angular orbits are shown in red.

slightly from the number of orbits for $\mu = 0.01$. We can then attempt to derive an expression for the number of orbits in the cases where μ is slightly larger than zero. This can be done by Taylor expanding the number of orbits found numerically to first order in μ , such that

$$N(\mu) = N(\mu = 0) + \mu N'(\mu = 0) + \dots \quad (3.49)$$

Here, the left hand side of the equation is the number of orbits calculated numerically and on the right hand side, $N(\mu = 0)$ is just equation (3.40). The final term on the right hand side is the contribution of the second primary body to the number of orbits needed to decrease C to C_1 . This assumes that for $\mu = 0$, the number of orbits calculated analytically should be equal to the number of orbits calculated numerically. Therefore, we can numerically integrate the equations of motion and calculate the second primary body contribution to the number of orbits by

$$\mu N'(0) = N(\mu) - N(0). \quad (3.50)$$

3.2.7 Controlling the precession

Using the Jacobi constant decreasing strategy outlined in section 3.2.3, an extended spacecraft can change C to be equal to C_1 , opening up a gap at L_1 to combine the two inner Hill regions. This allows the spacecraft to pass through the gap and orbit about the second primary body. However, the number of orbits calculated numerically and analytically for $C = C_1$ in sections 3.2.5 and 3.2.6, is only the number of orbits to open the gap in the Hill region. This does not give the number of orbits for the spacecraft to pass through the gap, which could be a significantly larger number of orbits. This is due in part to the fact that as the spacecraft orbits, the orbit precesses meaning the spacecraft may not orbit near enough to L_1 .

In the 2-body problem, choosing $q_+ + q_- = 0$, equation (3.26) vanishes and so the orbit does not precess. In the 3-body problem, the second primary body is a source of precession for the orbit of any spacecraft. As a result, setting the sum of the eigenvalues to be zero would still result in the orbit precessing. Therefore, to ensure that the orbit of the extended spacecraft performing the Jacobi constant decreasing strategy does not precess, we must measure the precession due to M_2 and choose $q_+ + q_-$ such that the total precession per orbit is zero.

If the total precession of the orbit is zero, then the orbit's major axis will extend towards L_1 as seen in figure 3.12. In this figure, we choose $\mu = 0.01$, $C_0 = 2C_1$. The black dashed line shows the orbits of a spacecraft with $q = q_+ = 0$ and $q = q_- = -(0.035)^2/12$ which we see are precessing. Then from this, we now choose the eigenvalues to be $q = q_+ = (0.035)^2/24$ and $q = q_- = -(0.035)^2/24$ which results in the blue orbit which does not precess.

Although $q_+ + q_-$ increases for the blue orbits, the difference, $q_+ - q_-$ is the same for the black dashed orbits and for the blue orbits. As the difference is the same, in both cases shown in figure 3.12, the number of orbits to decrease the Jacobi constant to C_1 is the same. For the non-precessing orbits, the

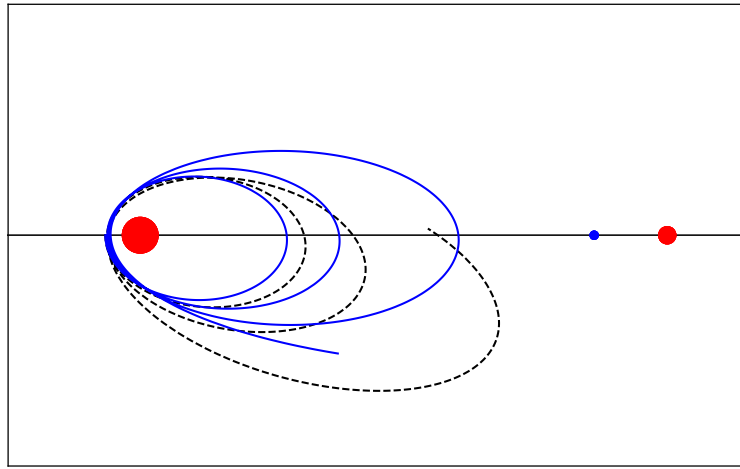


Figure 3.12: Example orbits showing how strategically choosing the sum of the eigenvalues ensures the orbit does not precess. In both the black dashed and blue orbit cases, $\mu = 0.01$, $C_0 = 2C_1$. The black dashed line has eigenvalues $q = q_+ = 0$ and $q = q_- = -(0.035)^2/12$. In this case, we then change the eigenvalues such that now for the blue orbits, $q = q_- = -(0.035)^2/24$ and $q = q_+ = (0.035)^2/24$. This ensures the difference between the eigenvalues remains the same but the sum of the eigenvalues is increased so that now, the blue orbit does not precess and instead, extends towards the blue dot, L_1 .

spacecraft will eventually orbit nearer to L_1 and should allow for it to pass through the gap in less orbits than in the precessing orbit case.

3.2.8 Stabilising

Having shown that an extended spacecraft can use extended body effects to change its eccentricity in the 2-body problem and its Jacobi constant in the 3-body problem, we now look at another application. As discussed in section 2.2.4, in the 3-body problem, there exists five Lagrange points. Using perturbation theory, we can approximately find the location of these five points to first order in μ and using these positions, we can calculate the derivatives of U to then evaluate the eigenvalues of \mathbf{A} . As shown in section, doing this for the three collinear points, we find that they are saddle points and are therefore unstable to perturbations from equilibrium [39].

We can then ask the question of whether or not using extended body effects could stabilise a spacecraft in the region about an unstable Lagrange point, using L_1 as an example. For a spacecraft with q equal to some constant, the four eigenvalues for L_1 will not all be purely imaginary. Therefore, some control law is needed to stabilise at the equilibrium point as a spacecraft with constant q cannot stabilise its orbit. Instead, much like the strategies developed for switching q to change the eccentricity or Jacobi constant, some strategy is required to stabilise about an unstable point.

Looking along the x -axis, there is a local maximum in the potential at L_1 and its location can be approximated using equation (3.41) to first order in μ . Then, allowing for extended body effects, we can approximate the x coordinate of L_1 to first order in μ and q . This can be done by first differentiating equation (3.35) with respect to x and evaluating at $y = 0$,

$$\frac{\partial U}{\partial x} = x - \frac{1 - \mu}{(x + \mu)^2} \left(1 + \frac{9}{2} \frac{q}{(x + \mu)^2} \right) + \frac{\mu}{(1 - x - \mu)^2} \left(1 + \frac{9}{2} \frac{q}{(1 - x - \mu)^2} \right).$$

At an equilibrium point, the derivatives of the potential must be equal

to zero so we first set $\partial U/\partial x = 0$ which when expanded, results in a ninth order polynomial in x . We then use the replacement $x \approx x_0 + qx_1$ and after this, we expand the polynomial and remove higher order terms involving q . The polynomial can then be written as $f_0(x_0, \mu) + qf_1(x_0, x_1, \mu) = 0$, then taking the second term and setting it equal to zero, we can derive an expression for x_1 in terms of x_0 and μ . To get x_1 only in terms of μ we use the replacement from equation (3.41) such that $x_0 = 1 - \left(\frac{\mu}{3}\right)^{\frac{1}{3}}$. Again, we remove higher order terms in μ and we are then left with, to first order in μ , $x_1 = -\frac{3}{2} \left(\frac{3}{\mu}\right)^{\frac{1}{3}}$. Combining this with equation (3.41), we can approximate the x coordinate of L_1 to first order and for non-zero q , as

$$L_{1,x} = 1 - \left(\frac{\mu}{3}\right)^{\frac{1}{3}} - q\frac{3}{2} \left(\frac{3}{\mu}\right)^{\frac{1}{3}}.$$

From this expression, it can be seen that changing the sign of q shifts the position of L_1 either side of L_1 for $q = 0$. We can use this fact as the basis for the control law. This shifting of the unstable equilibrium point depending on the value and sign of q results in figure 3.13, where the blue curve represents the potential evaluated with $q > 0$, the red curve is the potential with $q < 0$ and the black dashed curve is the potential for $q = 0$. The blue, red and black points represent L_1 for each potential curve.

From figure 3.13, by changing the sign of q either side of the black point, which is L_1 with $q = 0$, creates a potential well within which, a spacecraft could have a stable orbit. Therefore, we define the strategy to stabilise an extended spacecraft in the region about L_1 as:

1. $x < L_{1,x}$, set $q = q_+ > 0$.
2. $x > L_{1,x}$, set $q = q_- < 0$.

Recalling that the collinear equilibrium points are saddle points, an extended spacecraft with an initial position at L_1 , will be stable even with perturbations in only the y direction and therefore the spacecraft need only control q with regards to perturbations in x .

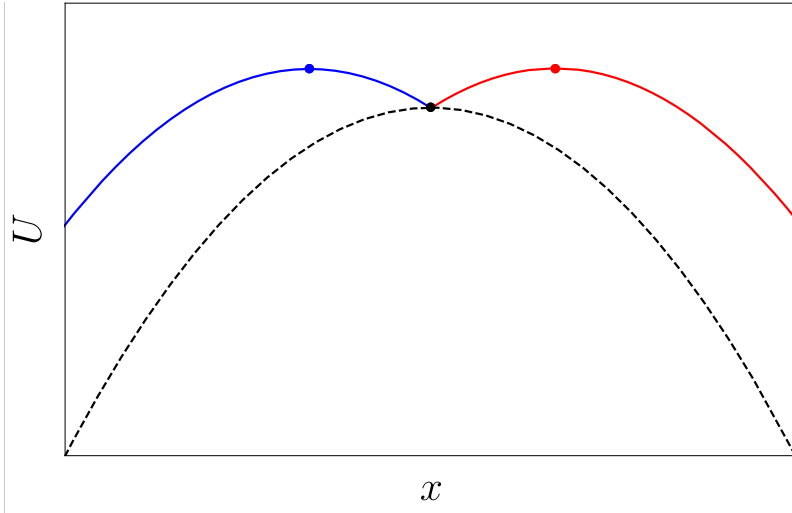
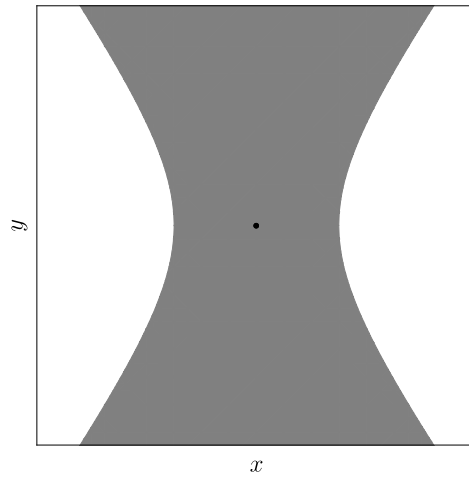


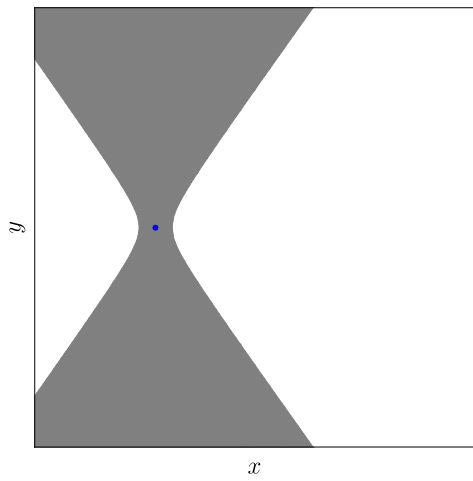
Figure 3.13: Potential curves for different values and signs of q . The blue curve represents the potential evaluated with $q > 0$, the red curve is the potential with $q < 0$ and the black dashed curve is the potential for $q = 0$. The blue, red and black points represent L_1 for each potential curve.

Using the strategy detailed, changing the sign of q changes U and as a result, changes the Jacobi constant of the spacecraft and subsequently the shape of the Hill region. As the spacecraft will be perturbed from L_1 , its Jacobi constant will be close to C_1 . If C is slightly larger than C_1 , the gap in the Hill region at L_1 will be closed. Then by changing the value of q , both the Jacobi constant and the Hill region changes in a similar manner to how the position of L_1 is moved. With C slightly greater than C_1 , L_1 with $q = 0$, is within the forbidden region between the two inner Hill regions. By changing q , L_1 moves and the forbidden region between the inner Hill regions moves with it. This can be seen in figure 3.14 for the cases of $q = 0$, $q > 0$ and $q < 0$.

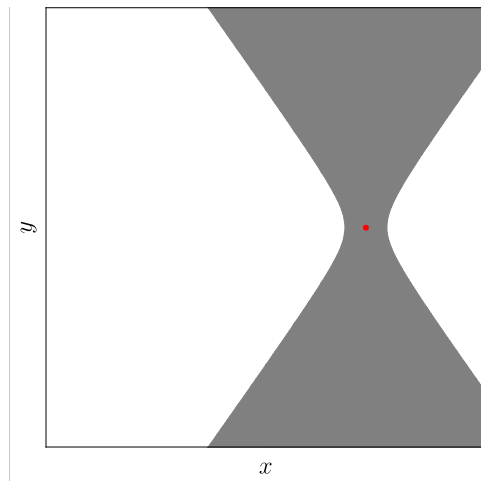
Combining figure 3.14b and 3.14c shows that by changing q using the strategy detailed, an enclosed Hill region is formed surrounding L_1 with $q = 0$. By choosing the initial conditions of an extended spacecraft such that $C_0 > C_1$ and perturbing it from L_1 with $q = 0$, it can be seen in figure 3.15 that this spacecraft will remain within this new enclosed Hill region as it will not be able to pass through the grey, forbidden region. Also shown in this figure are



(a) Hill region about the black point, L_1 , for an extended spacecraft with $q = 0$.



(b) Hill region about L_1 for an extended spacecraft with $q > 0$ with corresponding equilibrium point shown as a blue point.



(c) Hill region about L_1 for an extended spacecraft with $q < 0$ with corresponding equilibrium point shown as a red point.

Figure 3.14: Hill regions about L_1 for an extended spacecraft with C slightly greater than C_1 , with different values of q

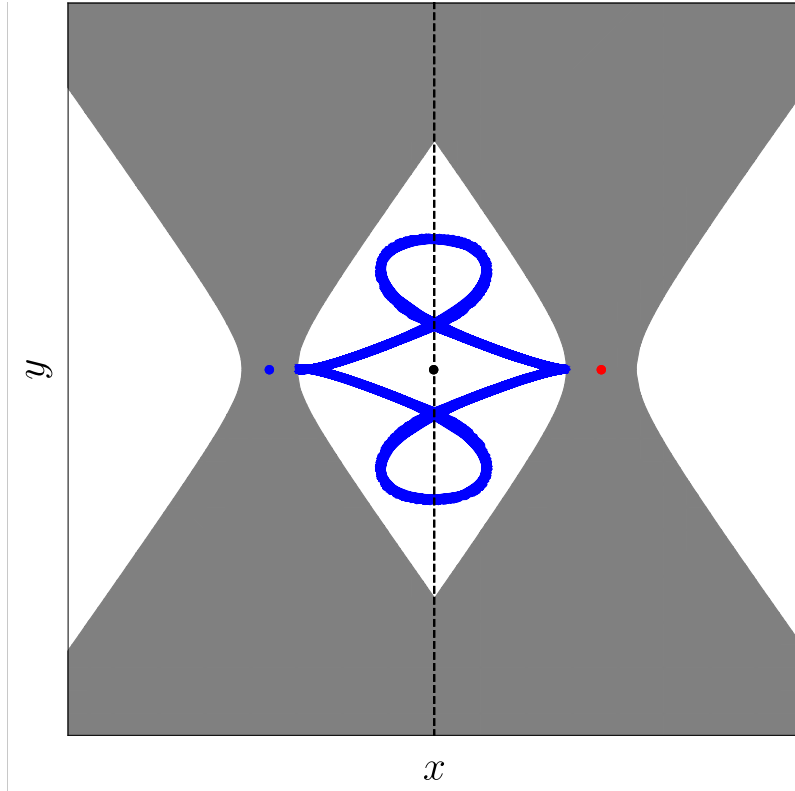


Figure 3.15: Orbits of an extended spacecraft within a Hill region about L_1 , created by switching the sign of q either side of the equilibrium point. The extended spacecraft has $q = q_+ = (0.02)^2/12$ and $q = q_- = -(0.02)^2/12$, with $\mu = 0.01$. The initial velocity of the spacecraft was set to zero in the rotating frame and it was then perturbed from the black point, L_1 . The blue and red points are the positions of L_1 when $q = q_+$ and $q = q_-$, respectively.

the orbits of an extended spacecraft with $q = q_+ = (0.02)^2/12$ and $q = q_- = -(0.02)^2/12$, with $\mu = 0.01$. The initial velocity of the spacecraft was set to zero in the rotating frame and it was then perturbed from the black point, L_1 .

3.2.9 Numerics

In figure 3.8, the number of instantaneous and angular orbits needed for the extended spacecraft to decrease C to C_1 is shown. This data is produced

using initial conditions $\mu = 0$, $C_0 = 2C_1$ and eigenvalues $q = q_+ = 0$ and $q = q_- = -(0.02)^2/12$. As $\mu = 0$, this is really just the 2-body problem. Using equation (3.40), we should find that this analytical result for the number of orbits, derived in the 2-body problem, should agree with the numerical data found in the 3-body problem using $\mu = 0$. We can see though from figure 3.10 that this is not the case and it is unclear as to where this disagreement arises from. Looking at figure 3.10, we see that the difference between the analytical and numerical results is largest when the initial orbit has eccentricity $e_0 = 0$, which occurs at the peak of the black dashed curve. Near the peak, with an initial radius of $r_0 = 0.56$, the difference in the number of orbits is $\Delta N \approx 3$.

The numerical data was produced using the automatically chosen integration method and tolerances for *NDSolve* so as a first test of the validity of the data, we can change the accuracy and precision goals of *NDSolve* and use the automatically chosen integration method. Accuracy is how close a measurement is to its true value and precision is how close multiple measurements are to each other [41]. The accuracy and precision goal specifies how many effective digits of accuracy and precision, respectively, should be found in the result of *NDSolve* [42].

By varying the accuracy goal while allowing *Mathematica* to automatically choose the precision goal, and then vice-versa, we can test whether the difference in the number of orbits converges to that of $\Delta N \approx 3$, the difference calculated in figure 3.10. We use the same initial conditions as in figure 3.10, so $\mu = 0$, $C_0 = 2C_1$, $q = q_+ = 0$ and $q = q_- = -(0.02)^2/12$ and now with initial radius $r_0 = 0.56$. The results of these tests are shown in figure 3.16. From this, we can see that increasing the accuracy and precision goal for *NDSolve* results in the difference in the number of orbits converging to the purple dashed line showing the difference in the analytical and numerical number of orbits from figure 3.10, which is $\Delta N \approx 3$.

We can then instead specify an integration method for *NDSolve* to use. A fixed step, Explicit Runge Kutta of order 2 was chosen and we vary the step size to test if ΔN converges to $\Delta N \approx 3$ as the step size decreases. The result of

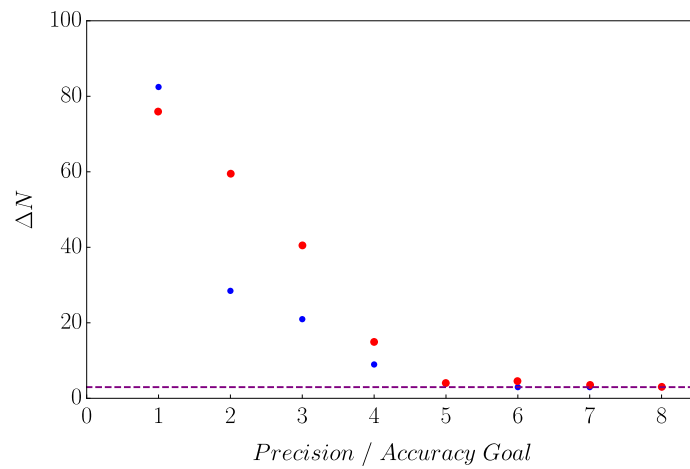


Figure 3.16: Difference between the analytical and numerical number of orbits for $C = C_1$ when changing the accuracy goal and allowing *Mathematica* to automatically choose the precision goal, shown in red. Shown in blue is the ΔN found by changing the precision goal and using the automatically chosen accuracy goal. Both data sets were found by directly numerically integrating the equations of motion, equation (3.32), using the integration method automatically chosen for *NDSolve*. The purple dashed line is the difference between the analytical and numerical number of orbits from figure 3.10, $\Delta N \approx 3$.

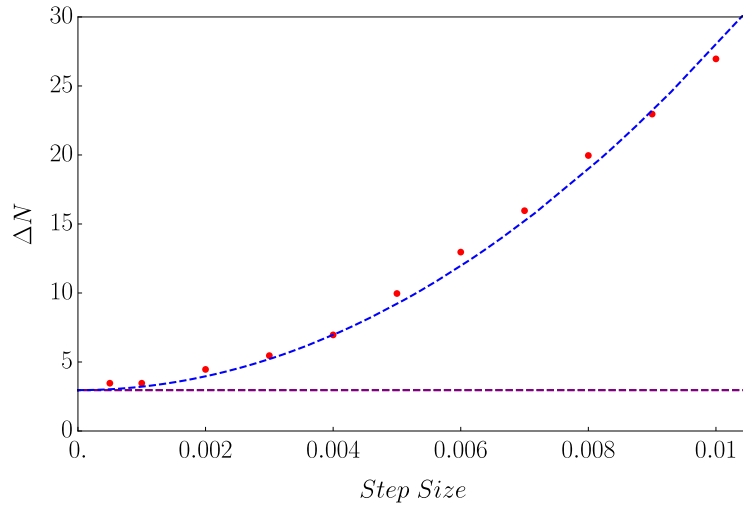


Figure 3.17: Difference between the analytical and numerical number of orbits for $C = C_1$ using a fixed step, Explicit Runge Kutta of order 2 for the integration method for *NDSolve*, while varying the step size, shown in red. The blue dashed line is proportional to $(\text{step size})^{\text{order}}$, where $\text{order} = 2$. The purple dashed line is the difference between the analytical and numerical number of orbits from figure 3.10, $\Delta N \approx 3$.

this is shown in figure 3.17. It is clear that decreasing the step size for *NDSolve* means the difference in the number of orbits converges to the difference in the analytical and numerical number of orbits from figure 3.10. The difference in number of orbits also increases proportionally to $(\text{step size})^{\text{order}}$, where $\text{order} = 2$, which is to be expected for the fixed step Explicit Runge Kutta integration method, when the step size is sufficiently small.

We can also perform these tests by looking at a more direct output of *NDSolve*. By directly numerically integrating the equations of motion, equation (3.32), *NDSolve* outputs the x and y coordinates of the spacecraft and so, for this test, we can choose to look at the radius of the spacecraft after 10 time units, $r(10)$. The same initial conditions were used to produce figures 3.16 and 3.17. First, we calculate $r(10)$ using the automatically chosen integration method and tolerances in *NDSolve* and this was found to be $r(10) = 0.5106$. By changing the accuracy goal, precision goal and then the step size, we can calculate the radius of the spacecraft after 10 time units and find the difference

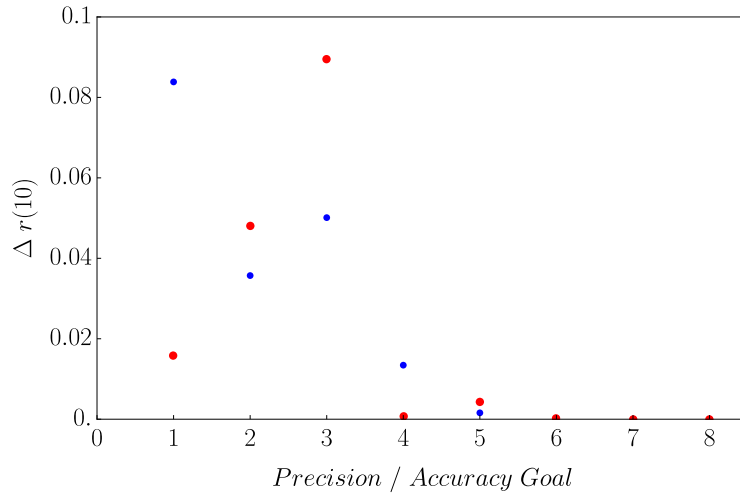


Figure 3.18: Difference between the position of the spacecraft after 10 time units, $r(10)$, using the automatic integration method and tolerances, and the same value found while changing the accuracy goal, shown in red, and precision goal, shown in blue, in *NDSolve*.

between this and the value found using the automatic method and tolerances, $r(10) = 0.5106$. This difference is given by $\Delta r(10)$.

In figure 3.18, we again see that increasing the accuracy and precision goal results in the difference between the data and the value found using the automatic method and tolerances, $r(10)$, converging to zero. Then using fixed step, Explicit Runge Kutta of order 2 again, we vary the step size and show that the difference in the calculated radius converges to zero as the step size decreases, as seen in figure 3.19. We also see that when the step size is sufficiently small, $\Delta r(10)$ is proportional to $(\text{step size})^{\text{order}}$, where $\text{order} = 2$.

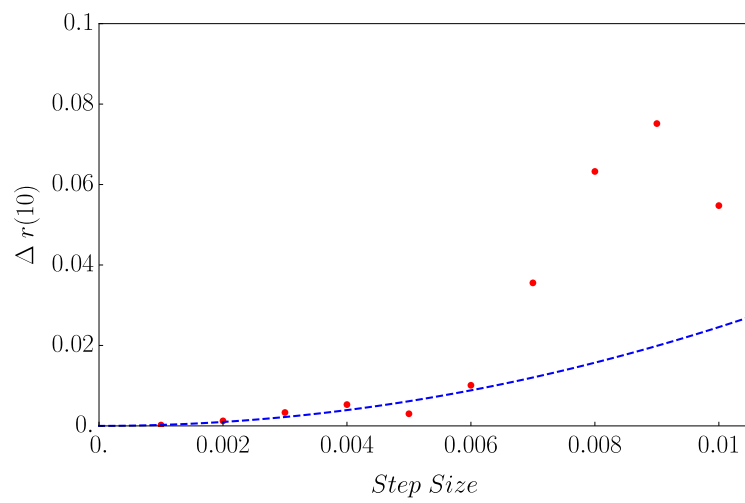


Figure 3.19: Difference between the position of the spacecraft after 10 time units, $r(10)$, using the automatic integration method and tolerances, and the same value found by varying the step size using a fixed step, Explicit Runge Kutta integration method in *NDSolve*. When the step size is sufficiently small, $\Delta r(10)$ is proportional to the blue dashed line which is given by $(\text{step size})^{\text{order}}$, where $\text{order} = 2$.

Chapter 4

Conclusions

4.1 Discussion

It is clear that in the 2 and 3-body problem, there are a number of fuel-free possibilities for a spacecraft which uses extended body effects strategically. In contrast to the current literature [10–15], no specific model for the extended spacecraft was adopted here and instead, we show that the relevant details of a spacecraft can be described using its quadrupole moment. Doing this allows us to see that for the torque on an extended spacecraft to vanish, the radial vectors must be eigenvectors of the quadrupole moment, as seen in equations (2.21) and (2.25) and this has not been demonstrated previously. Preventing the extended spacecraft from spinning up is an important feature of the design of the spacecraft and this is usually done using reaction wheels or allowing the transfer of angular momentum from spin to orbital angular momentum [10, 12, 13]. As was discussed in section 3.1.1, even a small change in orbital angular momentum will result in a large change in the spin angular momentum which could result in the spacecraft spinning up and possibly tearing itself apart.

As mentioned, the problem of motion of an extended spacecraft has been discussed in the 2-body problem but has not, to the author’s knowledge, been

discussed in this way in the 3-body problem. We show here that an extended spacecraft can make changes to its orbit without the use of a reaction mass and instead of only numerically integrating the equations of motion, we also look more directly at the changes in energy and Jacobi constant and show how they relate to changes in the spacecraft's mass distribution.

4.1.1 2-body problem

An extended spacecraft can control its orbit using extended body effects. By Taylor expanding the gravitational field from a primary body, we can move away from the point particle approximation to now include the quadrupole moment of the mass distribution, Q^{ij} . Then, to ensure an extended spacecraft does not spin up, we see that equations (2.21) and (2.25) vanish when the radial vectors are eigenvectors of Q^{ij} . By using the eigenvector condition, we can then define a single control parameter which is the eigenvalue, q of Q^{ij} . This control parameter is time dependent and its sign is unconstrained which allows for a number of possibilities when orbiting in the 2 and 3-body problem.

In the 2-body problem, the energy of a point particle is conserved but it was shown that allowing for extended body effects means the energy of an extended spacecraft can change over time by strategically changing q . Changing the energy also leads to a change in the eccentricity of the spacecraft and so, an extended spacecraft can change its orbit between two eccentricities by strategically changing the value of q , as described by the strategies detailed in section 3.1.2. This change in eccentricity per orbit depends on the difference between the minimum and maximum values of the eigenvalues, q_- and q_+ . Solving the differential equation for the change in eccentricity allows it to be written as a function of the number of orbits about the primary body, $e(N)$. From this, we can find the number of orbits needed to change eccentricities between some initial and final value.

While undergoing the strategy of switching q to change the eccentricity, the orbit of the extended spacecraft also precesses. This is not the case

in the point particle approximation as stated in Bertrand's theorem. Using the Laplace-Runge-Lenz vector which points towards the instantaneous pericentre, we can measure the orbits precession per orbit while undergoing the eccentricity increasing strategy. Now in this case, it was shown that the precession angle per orbit is constant and depends on $q_+ + q_-$. This is in contrast to the change in eccentricity and therefore with particular choice for q_+ and q_- , we can ensure that the eccentricity of the orbit of an extended spacecraft increases while the orbit does not precess, as shown in figure 3.5.

Some examples of the different designs of extended spacecraft were also discussed. In the basic example, it was shown that a barbell shaped spacecraft can vary the length between two point masses to vary the magnitude of the eigenvalue. Then to change the sign of q , we discussed the design of an extended spacecraft similar to that of the barbell but now with two hoops instead of point masses. By varying the length between the hoops and the radius of the hoops, both the magnitude and the sign of q can be controlled.

4.1.2 3-body problem

In the planar, circularly restricted 3-body problem, it was once again necessary to first ensure that an extended spacecraft was torque-free. Even with the introduction of a second primary body, the eigenvector condition can still be used as there are two degenerate eigenvalues of Q^{ij} , corresponding to an infinite number of pairs of eigenvectors which do not need to be perpendicular to one another. This allows both radial vectors for the two primary body to be eigenvectors of Q^{ij} simultaneously, ensuring the extended spacecraft is torque-free and once again, we can use a single control parameter, q . We can also simplify the problem by non-dimensionalising the equations of motion. In this problem, the Jacobi constant is the only known conserved quantity. Much like the energy in the 2-body problem, by allowing extended body effects, the Jacobi constant can be decreased over time by strategically changing q using the strategy detailed in section 3.2.3.

For an extended spacecraft with an initial Jacobi constant C_0 greater than C_1 , the Jacobi constant at Lagrange point one, the inner Hill region is separated in two, with one Hill region surrounding each primary body. The forbidden region between the two inner regions surrounds L_1 and by decreasing C_0 such that $C < C_1$, a gap opens in the forbidden region and the two inner Hill regions combine. This allows the spacecraft to pass through the gap at L_1 so as to transfer its orbit from one primary body to another. Once it passes through, the spacecraft could then change strategies so as to make $C > C_1$ which closes the gap at L_1 again. The changes in Hill region shapes were shown in figure 2.4.

By showing an extended spacecraft can change its Jacobi constant to allow some orbital manoeuvres, the question of how many orbits was needed to decrease C to C_1 was discussed. The number of orbits needed to change between two eccentricities as derived in the 2-body problem was used as the analytical result for the number of orbits for $C = C_1$ in the 2-body limit of the 3-body problem, or, as $\mu \rightarrow 0$. When compared to the number of orbits calculated numerically from direct numerical integration of the equations of motion, a disagreement between the analytic and numerical results was found. There were a number of solutions explored so as to try eliminate this discrepancy however all were unsuccessful.

In contrast to the 2-body problem, in the 3-body problem, even the orbits of a point particle precess due to the introduction of the second primary body. In the 2-body problem, if the sum of q_+ and q_- is chosen to be zero, then the orbit does not precess. However, in the 3-body problem, we can instead strategically choose $q_+ + q_-$ so that it negates the precession from M_2 and so the orbit of an extended spacecraft will not precess. This can be used in the Jacobi constant decreasing strategy so as to allow the orbit to extend towards L_1 , thus decreasing the number of orbits needed for the spacecraft to pass through the gap in the Hill region.

Finally, it was shown that extended body effects could be used to stabilise a spacecraft in the region about an unstable point, using L_1 as an ex-

ample. By strategically varying the sign of q , the position of the equilibrium point is shifted either side of L_1 which results in the creation of an enclosed Hill region about L_1 , within which a spacecraft can have a stable orbit. The orbits of an extended spacecraft in the region about L_1 are shown in figure 3.15, which were found by numerically integrating the equations of motion. The orbits shown are of an initially perturbed extended spacecraft following the strategy for switching the sign of q either side of L_1 and it is shown that periodic orbits can exist within the created enclosed Hill region.

4.2 Future perspectives

While it was shown that using extended body effects can allow for a spacecraft to perform fuel-free manoeuvres, there are a number of areas for further research. The first and most important would be to solve the disagreement between the numerical and analytical results for the number of orbits for $C = C_1$. Solving this disagreement would allow for the number of orbits to be calculated in low mass ratio 3-body systems, using equation (3.50).

The numerical results for the number of orbits and the orbits of a spacecraft stabilising itself about L_1 were also derived using the automatically chosen values for precision and accuracy goals and integration method for *NDSolve* in *Mathematica*. In section 3.2.9, some basic tests were performed to investigate the validity of the numerical results. These tests showed that by increasing the accuracy and precision goal for *NDSolve*, the difference between the analytical and numerical number of orbits and the radius of the spacecraft after 10 time units converges to the results found using automatically chosen values for the accuracy and precision goal.

Then a fixed step, Explicit Runge Kutta integration method was used for *NDSolve*. It was shown that by decreasing the step size for the numerical integration in *NDSolve*, the results again converged to those found using the automatic integration method. So while these do not explain the difference be-

tween the analytical and numerical number of orbits shown in figure 3.10, these initial tests show to some degree that the numerical results can be trusted. An area for future research would be to perform more rigorous convergence tests to fully test the validity of the numerical results.

As shown, a spacecraft can use extended body effects to perform a number of orbital manoeuvres in Newtonian gravity. There are also many possibilities not discussed here that could be developed. In both the 2 and 3-body problem, we assumed that the primary bodies were spherically symmetric which is only an approximation, much like assuming all spacecraft are point particles. In the 2-body problem, the problem of stabilising the orbit of an extended spacecraft about an oblate primary body has been discussed [37] and so the motion of an extended spacecraft about two oblate primary bodies could also be investigated.

At the beginning of the discussion of the 3-body problem, we assumed the problem could be simplified to the planar, circularly restricted problem. While the circularly restricted problem is a good approximation, at least for most planets in the solar system [43], we could step away from the planar motion problem and allow for motion of an extended spacecraft out of the orbital plane of the primary bodies. Finally, we have discussed only the motion of an extended spacecraft in Newtonian gravity. However, it is also possible to discuss extended body motion in general relativity [44].

Bibliography

- [1] D. A. Shearer and G. L. Vogt, “Rockets educator’s guide,” 2020.
- [2] I. Newton, *Philosophiæ Naturalis Principia Mathematica*. Edmund Halley, 1687.
- [3] D. R. Williams. “Specific impulse.” (2015).
- [4] M. Meyer *et al.*, *In-Space propulsion Systems roadmap*. NASA, 2012.
- [5] A. Jones. “Three decades in the making, china’s space station launches this week.” (2021).
- [6] E. Behrend. “Starlink mission.” (2019).
- [7] S. D. Clark, “Bepicolombo electric propulsion thruster and high power electronics coupling test performances,” 2013.
- [8] D. Brown. “Nasa’s dawn mission to asteroid belt comes to end.” (2018).
- [9] J. L. Wright, *Space Sailing*. Gordon and Breach Science Publishers, 1992.
- [10] G. A. Landis, “Reactionless orbital propulsion using tether deployment,” 1992.
- [11] V. V. Beletsky, “Essays on the motion of celestial bodies,” 2001.
- [12] J. Gratus and R. Tucker, “An improved method of gravicraft propulsion,” 2003.
- [13] M. J. Longo, “Swimming in newtonian space–time: Orbital changes by cyclic changes in body shape,” 2004.
- [14] C. Murakami, “On orbit control using gravity gradient effects,” 1981.

- [15] M. Martinez-Sanchez and S. A. Gavit, “Orbital modifications using forced tether-length variations,” 1987.
- [16] Y. Chen *et al.*, “History of the tether concept and tether missions: A review,” 2013.
- [17] J. Peláez and D. J. Scheeres, “A permanent tethered observatory at jupiter. dynamical analysis,” 2007.
- [18] J. Peláez *et al.*, “Dynamics and stability of tethered satellites at lagrangian points,” 2008.
- [19] R. M. Canup, K. M. Kratter, and M. Neveu, “On the origin of the pluto system,” 2021.
- [20] A. Einstein, “Die grundlage der allgemeinen relativitätstheorie,” 1916.
- [21] E. Poisson and C. M. Will, *Gravity: Newtonian, Post-Newtonian, Relativistic*. Cambridge University Press, 2014.
- [22] M. J. Bertrand, “Théoremè relatif au mouvement d’un point attiré vers un centre fixe,” 1873.
- [23] H. Goldstein, C. Poole, and J. Safk, *Classical Mechanics*. Addison Wesley, 1980.
- [24] J. A. Shapiro, *Classical Mechanics*. J. A. Shapiro, 2010.
- [25] I. Newton, “Philosophiae naturalis principia mathematica,” 1687.
- [26] Z. E. Musielak and B. Quarles, “The three-body problem,” 2014.
- [27] R. L. Heacock, “The voyager spacecraft,” 1980.
- [28] W. S. Koon, M. W. Lo, J. E. Marsden, and S. D. Ross, *Dynamical Systems, the Three-Body Problem and Space Mission Design*. Marsden Books, 2006.
- [29] NASA. “International space station main systems.” (2015).
- [30] J. E. Barrow-Green, *Poincaré and the Three Body Problem*. PhD thesis The Open University, 1993.
- [31] J. L. Synge and B. A. Griffith, *Principles of Mechanics*. McGraw-Hill Book Company, 1942.

- [32] C. G. J. Jacobi, “Sur le mouvement d’un point et sur un cas particulier du problème des trois corps,” 1836.
- [33] S. H. Strogatz, *Non Linear Dynamics And Chaos*. Westview Press, 2015.
- [34] N. J. Cornish, “The lagrange points,” 1998.
- [35] G. W. Hill, “Researches in the lunar theory,” 1878.
- [36] E. Belbruno, *Capture Dynamics and Chaotic Motions in Celestial Mechanics*. Princeton University Press, 2004.
- [37] A. Harte and M. Gaffney, “Extended-body effects and rocket-free orbital maneuvering,” 2021.
- [38] H. P. Langtangen and G. K. Pedersen, *Scaling of Differential Equations*. Springer, 2016.
- [39] N. J. Cornish, “The lagrange points,” 1998.
- [40] T. Logsdon, *Orbital Mechanics: Theory and Applications*. John Wiley & Sons, 1997.
- [41] Presica. “What is the difference between accuracy and precision measurements?” (2022).
- [42] Wolfram. “Wolfram language & system documentation center.” (2022).
- [43] D. R. Williams. “Planetary fact sheet - metric.” (2019).
- [44] A. I. Harte, “Extended-body effects in cosmological space-times,” 2007.